POLITECNICO DI TORINO

Master's Degree in Mechatronic Engineering

Master's Degree Thesis

Analysis on the installation of long-range radar sensors in modern vehicles

Supervisors

Prof. Nicola AMATI

Prof. Francesco Paolo DEFLORIO

Candidate

Massimiliano MISCIA

December 2022

Abstract

The thesis focuses on radar sensors used in automotive industry, understanding the principle of operation, evaluating their installation and positioning in the front bumper of a car and testing their ability to work in representative scenarios. In particular, the mechanical aspects related to the packaging and installation of the radar sensor are considered, reasoning about the constraints of the materials and geometry of the radar cover and the bumper. Considerations about the mounting position are derived from simulations and the study of the pros and cons of carmaker's solutions. The thesis deals with analysis of representative scenarios and a corner case, the cut-in maneuver, in which the radar could be, evaluating its ability to perceive the surrounding environment.

Table of Contents

List of Figures

List of Tables

Chapter 1

1. Introduction

An advanced driver-assistance system (ADAS) assist drivers in driving and parking functions. Through a safe human-machine interface, ADAS increase car and road safety. These systems use automated technology, such as sensors, to detect nearby obstacles or driver errors, and respond accordingly.

To achieve these goals combination of different sensors is needed but, leveraging on their main characteristics, radar sensors are among those more used especially for long range detection purposes. The thesis deals with this sensor, explaining how it works and how it is integrated in a car, reasoning about the material, geometric and positioning constraints related to its installation.

The content of each chapter is briefly summarized. In chapter 2 an introduction to the advanced driver-assistance systems (ADAS) is done, presenting the main solutions available on the market, understanding their aims and how these systems work. In particular, attention is put on the Adaptive Cruise Control, the Autonomous Emergency Braking, the Blind Spot Detection, the Cross Traffic Alert, and the Park Assistant. In chapter 3 is given a description of the main sensors used to perceive the surrounding environment and so to provide to the ADAS algorithms inputs to be elaborated in order

to reach the desired goal. For each of these sensors (camera, lidar, radar and sonar) a brief explanation is given underlining their pros and cons. Chapter 4 goes in deep on the functioning of automotive radars evaluating how they can provide information about range, velocity and angle of arrival of the observed targets. The frequency modulated continuous wave radars (FMCW radars), that are the most used in the automotive field, are treated, deriving mathematically the main equations that characterize them. Since the electromagnetic waves sent by the automotive radar have a proper range of frequency to work on, in chapter 4 also the allocated frequency bands and their effects on the transmission are mentioned, considering that from 2022 the band used for short range detection radars changed and so a comparison with the used previously is done. Chapter 5 shows how the integration of the radar in the car is performed, focusing mainly on long range detection radars usually installed in the front bumper. Since they are covered by different material layers, in chapter 5 also the main constraints that have to be taken into account when design these covers are presented, in order to provide a design guideline. In chapter 6 are done analysis and simulations about the multi-layers structure in which the radar is integrated, in order to evaluate the power losses and the attenuation introduced by the installation on the car. Since these covers and the bumper itself may have a certain shape in the area in which the radar is mounted that can be curved, chapter 7 evaluates instead the angle error and so how much radar beams are deflected when passing through curved surfaces. Finally in chapter 8 reasonings about the position of the radar in the front bumper are done, analyzing with an AV simulator software the effect of a position shifting both in an ordinary scenario in which radar can work and in a corner case, the cut-in maneuver, which is a critical one and among those in which a different positioning most influences the desired performances.

Chapter 2

2. Advanced Driver-Assistance Systems

An advanced driver-assistance system (ADAS) is a set of technologies that help drivers in guiding and parking operations [1], [2]. ADAS improve vehicle and road safety. These technologies use sensors to perceive nearby obstacles or driver mistakes and react accordingly. ADAS can guarantee different degrees of autonomous driving, according to the features installed in the car. A lot of accidents are caused by human errors, for this reason vehicles are equipped with ADAS that automate and improve technologies better driving and safety. Safety features are designed to avoid crashes and collisions by alerting the driver to issues, implementing safeguards, and seizing control of the car if indispensable. In the following paragraphs, a description of these systems is given, focusing mainly on the ones that need to perceive also external inputs.

2.1. Adaptive cruise Control

The adaptive cruise control, also known by the acronym ACC, was launched for the first time in 1995 by Mitsubishi, which integrated it (with laser sensor) on the Diamond, a

car model addressed for the Japanese market, while the first ACC that takes advantage from radar sensor, was introduced by Toyota in 1997 and later by Mercedes in 1998. Since then, this system has widespread to different medium-high cost cars and in fact represents an essential step towards the self-driving cars of the future (autonomous vehicles). The ACC is an electronic control system that handles the velocity of the car on which it is integrated. It is so a system able of adapting the cruising speed, raising or lowering it, in accordance with traffic conditions. The prerogative of this ADAS is the efficiency in constantly preserving the right safety distance with the vehicles in front. If for example, the car in front in your lane suddenly slowed down, the system would understand it in a few thousandths of a second and would respond accordingly, adjusting the speed. This guarantees a higher safety since the reaction time of the device is much less than that of any driver, who on average reacts in one second. The same device is also known as dynamic cruise control. The control is based on the information provided by the on-board sensors. A radar or laser allows the system to brake the vehicle when it is approaching another one in front, and then accelerate when traffic allows. Nowadays most ACC systems are radar-based leveraging on the properties of these sensors and on the fact that they can be hidden behind plastic covers, without compromise the aesthetic design of the car. For example, Mercedes Benz mounts the radar in the center of the front grille concealed by a molded and painted plastic fascia to reproduce the look of the rest of the grille. ACC is considered a key component for next generations of intelligent vehicles. They influence the safety and comfort of the driver, as well as the smoothness of traffic, by keeping an optimal distance between vehicles and lowering the probability of driver error. Vehicles equipped with adaptive cruise control are considered autonomous level 1, according to the SAE international classification. If combined with another driver assistance system such as the lane keeping one, it permits the car in question to reach level 2 of automation. Adaptive cruise control does not provide complete autonomy: the technology only guarantees assistance to the driver, it does not guide the vehicle autonomously, but by activating the ACC the driver will no longer have to intervene on the pedals if not for take control when needed. Should the accelerator, clutch or brake be pushed, the system will be turned off and the driver will take again control of the vehicle. In addition, ACC can be deactivated by the same activation button. Precisely for this reason, this system was

thought for high-traffic road sections, since in an urban environment, where actions on the pedals are much more common, the Adaptive Cruise Control would be deactivated continuously. The differences between the classic cruise control and ACC are that even if both are thought for highway and high-traffic travels and their common aim is to maintain the desired speed, the Classic Cruise Control is a driving assistance system that, once activated, preserve the set speed, regardless of external scenarios. Therefore, it demands the necessary intervention of the driver to increase speed or decelerate. Adaptive Cruise Control has resolved this problem, since it is able to preserve the set cruising speed, but also modifies the performance of the car based on external circumstances.

ACC can manage the actuators that act on the brakes, accelerator and automatic gearbox (if present), with an average range of action between 30 and 180 km/h. In addition, some Accs permit the complete stop of the vehicle, independently handling (within predetermined times) even the restart phases.

Another version is the i-ACC, the adaptive control of the intelligent cruise speed that also reveals the speed limits showed by road signs, giving the driver the possibility to reset the car's velocity to the new limit simply by using the controls on the steering wheel.

Compared to the basic Acc, then, the i-Accs complete the sensors with the presence of cameras, mounted behind the windshield and, sometimes, on the sides of the vehicle, the data of which are combined with that given by the radars.

The speed limit can, for example, be determined by software that examines images given by the camera and recognizes vertical signs.

Once the speed is set, if the system recognizes a lower limit signal, it automatically decreases the vehicle's velocity accordingly, resuming the preset speed once a new signal is detected. This function, however, can be turned off, this can be useful if traveling on roads where the limit signs are arranged in a disorderly manner, as sometimes happens in the presence of road construction sites.

2.2. Autonomous Emergency Braking

Many accidents are caused by late use of the brakes or not adequate braking force. The driver may brake late for a number of reasons: he may be overtired or distracted, or he could be in conditions of poor visibility due to different environmental conditions. In other cases, there may not be the time necessary for the abrupt and unexpected braking of the car in front. Most people are not prepared for such circumstances and do not apply the necessary braking to avoid a crash. Some manufacturers have introduced systems that assist the driver avoid this kind of accidents, or at least lower their seriousness. The technologies can be grouped in the Autonomous Emergency Braking (AEB) category.
Many AEB systems take advantage of a combination of radar and camera sensors that are either mounted at the front of a car or installed inside the windshield.
AEB was introduced in 2009 by Volvo and it worked by using mainly radars to evaluate the distance to any vehicle, pedestrians and other obstacles in front, and then responds if that distance abruptly decreases at a great rate, usually because the object in front has come to, or is coming to, a sudden stop. Its name describes properly the system:

- Autonomous: act independently of the driver to avoid or moderate the consequences.
- Emergency: they intervene only in a critical situation.
- Braking: they try to avoid the crash by braking.

AEB systems increase safety in two different ways: first, they give an help by identifying crucial circumstances in time and warning the driver; secondly, they decrease the seriousness of unavoidable crashes, lowering the collision speed and, in some cases, preparing the car and seat belts for impact.
If it perceives a potential accident, the AEB first (but not always) tries to prevent the crash by warning the driver to the necessity to take corrective action. If the driver does not intervene and the collision is coming, the system applies braking. Some systems guarantee a full braking, others partial braking. The AEB can also add braking force if the driver is pushing down the brake, but weaker than the car needs to avoid the impact. In any case, the aim is to decrease the collision speed. Some systems are turned off

when the driver takes corrective action. The AEB system will evaluate the needed braking force to be used. Different AEB systems have different operating speed ranges and there are diverse types of hazards they can recognize. For example, some AEB are more efficient in low velocities urban areas, while others are better equipped to manage rural or multi-lane driving.

2.3. Blind Spot Detection

Failing to see the car approaching suddenly from behind in the left-hand lane or in the blind spot of the car happens very often, especially in congested traffic on multi-lanes highways as well as in urban traffic scenarios.
The Blind Spot Detection (BSD) system can observe this area and relieves much of the driver's efforts and avoid dangerous situations. Using a video camera or radar, BSD is a vehicle-based sensor device that perceives other vehicles located to the driver's side and rear. Warnings can be visual, audible, vibrating, or tactile. This system was first introduced on the Volvo XC90 SUV and provided a visible warning when a car went inside the blind spot when a driver was changing lanes, taking advantages from cameras and radar sensors placed on the door mirror housings to check the blind spot area. Volvo won an AutoCar Safety and Technology award for the implementation of this feature. BSD systems mainly use medium range radars (MRR) set in the rear and side of the car. These radars perceive vehicles present in the so-called blind spot, that is that cone of visual shadow between the central rear-view mirror and what is visible from the side rear-view mirror. There are mainly two types of BSDs, passive and active. Passive BSD systems only alert the driver to the presence of a vehicle in the blind spot. The radar recognizes the presence of the car and, through the vehicle can line, sends signals to the driver. The most common signals are made through the turning on of alerting lights generally placed on the exterior rear-view mirrors or on the front interior pillars. With BSD the chances of a collision due to a lane change are consequently reduced. Active BSD systems have the same operating principle as passive ones but integrate communication with the engine control unit and the ABS control unit. When the driver starts to change lane and the radar discover the presence of a car in the blind spot, the

technology intervenes on the engine control unit by cutting power and on the ABS control unit by braking the opposite front wheel to avoid the lane change. In this case we have an intervention of the ADAS system on several control units at the same time and the collision is almost always avoided.

2.4. Cross Traffic Alert

Cross Traffic Alert (CTA) helps to see what the human eye cannot see [3]. By perceiving possible hazardous circumstances, the system improves driving safety by diminishing the risk of collisions due to the low visibility of car's surroundings. Cross Traffic Alert is an active safety system. It uses radars and often cameras to perceive obstacles and then alert the driver of the imminent approach of a car. When CTA detects a potentially dangerous circumstance, it warns the driver with light signals, mounted on the rear-view mirrors, and sound. The sensors, observing the obstacle in advance, predict a possible crash in a short time and warn the driver of the danger, who must immediately interrupt the maneuver. When the area becomes again free, the signals will stop, allowing the driver to continue the maneuver. Front Cross Traffic Alert, shown in Figure 2.1, detects vehicles passing in front and warns the driver. Using front lateral side radar, Front Cross Traffic Alert perceives crossing obstacles around 50 m ahead. A warning can be sent to the Head-up Display to show the other car's position. If the driver continues to move towards crossing cars, audio alerts will sound to allow the driver to stop in time.

Figure 2.1: Front Cross Traffic Alert example, from [3]

Rear Cross Traffic Alert [4] is a complementary support to BSD that helps the driver to detect vehicles traveling transversely behind the car when reversing. The automatic braking sub-function can help the driver stop the car if there is a risk of accident. CTA is thought to first detect vehicles. Under favorable circumstances it can also perceive smaller objects such as bicycles and pedestrians. It is very useful for assist exit maneuvers from vertical parking as shown in Figure 2.2. It often starts working at speeds over 10 km/h and it can identify cars traveling up to 20 km/h less and 70 km/h more than the vehicle on which it is installed. Unlike many ADAS, the Rear Cross Traffic Alert does not desire any manual insertion but is turned on automatically when reverse gear is engaged.

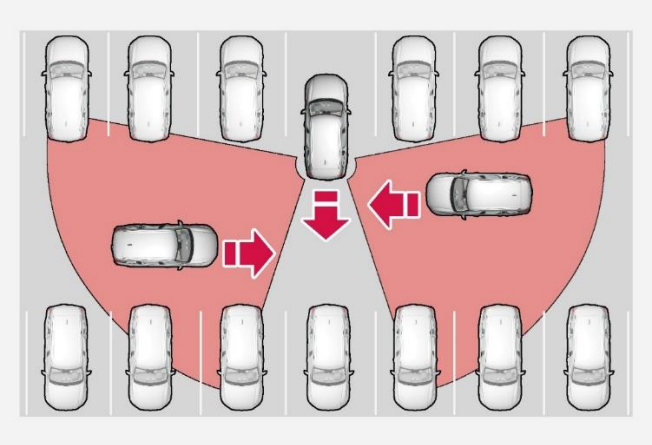

Figure 2.2: Rear Cross Traffic Alert example, from [4]

2.5. Park Assistant

The Parking Assistant or semi-automatic parking is a system able of actively assisting the driver in parking maneuvers. It was first installed on the Toyota Prius in 2003. It autonomously handles the search for parking, the evaluation of the required space and the steering maneuvers, but does not control the throttle control, the gearbox and the brakes, which must in any case be managed by the driver. The system is known under several names, in base on the manufacturer or the car manufacturer that makes it. Park Assist permits to park the vehicle in spaces parallel to the road and also perpendicular. It

assists the driver in finding suitable longitudinal and transverse parking spaces. After the driver has turned on the system, it starts scanning both sides of the carriageway (both left and right, for example in a one-way street), searching for any free parking spaces. At this stage, in fact, if the car is moving at low velocities (usually up to 40 km/h) and at a limited distance from the roadway, the system monitors the free space between the cars already parked while the vehicle passes by (mainly ultrasonic sensors are used, but it can be done also by radar sensor). By turning on the direction indicator, the driver determines the side of the road where he wants to leave the car. When the park assistant finds a space at least 80 centimeters longer than the car (on the first-generation systems, at least 1.20 meters was required), a message is displayed. The driver is then moved to the correct position to start the parking maneuver. The first step to take is to engage reverse gear. At this point the driver will have to properly handle the gas, while the parking assistant will steer the car totally autonomously. If the driver intervenes or the steering is turned, the system switches off. The end of the reverse maneuver is indicated by an acoustic signal. Additional images on the display tell the driver to move forward and, if required, to engage reverse gear again. The number of parking maneuvers depends on the length of the parking lot. The smaller this lot is, the more parking maneuvers will be required. The system also helps the driver when exiting the parking spaces. It is however possible to intervene and turn off the Park assist when desired. The second-generation systems are able to guarantee assistance also in herringbone car parks. Furthermore, are already available park assists that can handle the parking maneuver completely excluding the driver's intervention, but at the present time they are not put on the marked also for any issues of attribution of responsibility in the case of a collision with other cars (the driver would in fact be decommissioned). The semi-automatic parking system is quite widespread, since it is also present on medium-cost vehicles, where it is usually available as an option. Among the main limits, there is the space required to carry out the maneuver. It almost always is very large and with the possibility that the parking lots in which a good driver would be able to park, will be ignored by the system because they are considered small.

Chapter 3

3. ADAS Sensors

In the previous chapter the main advanced driver-assistance systems were presented and the starting point for all of them is make the car able to correctly perceive the surrounding environment. Perception is a key component in automation and driving assistance and is performed through different sensors, each of them with its peculiarities, pros and cons. Moving towards completely autonomous vehicles integration and coexistence of different sensors such as cameras, lidars, radars and ultrasound sensors in necessary to guarantee awareness of the environment and vision from different point of view, putting together the advantages deriving from each of them. In the following paragraphs the main characteristics and limits of these sensor are presented [5], [6].

3.1. Camera

Cameras are sensors able of capturing an image, converting it into an analog electrical signal and consequently transform into digital information. Cameras, like the one shown

in Figure 3.1, are placed outside the vehicle on the front, back and sides to take images of the street signs, road, vehicles, pedestrians and other obstacles. They are useful to perceive, obstructions, read lines and other markings on the road, recognize traffic sign and much more. They can also be used for other purposes like security and rain detection as well.

Figure 3.1: Camera sensor, from [5]

Captured images are examined by supporting software and the information then triggers a response to improve safety. This could be alerting the driver that he is leaving the lane or that there's a car in the blind spot, or helping him park the car. The ADAS systems that leverage on cameras are programmed to process the stream of images and, for example, understand that another vehicle is signaling a right turn, to identify stop signs and that a traffic light has just turned red, yellow or green and more. This is a huge amount of data and required processing power, and it's only increasing in the march toward self-driving cars. Cameras are less powerful when is required to see in the dark, or when the air is dense with fog, rain, snow, etc. They also require a lot of processing power.
The camera features can be resumed as follow:

• It is low priced;
• It has the highest resolution between all sensors, as it is able to capture a large quantity of information;
• It produces a large quantity of data, therefore it requires deep learning;

• Imitates the functioning of the human eyes;
• It is not reliable in adverse climatic circumstances.

3.2. LiDAR

LiDAR is the acronym of Light Detection and Ranging. The sensor permits to detect the distance to an object using a laser pulse. The distance is measured by sending the laser or light beam to the surface and evaluating the time it takes to come back.

Figure 3.2: LiDAR sensor, from [5]

LiDAR sensors, like the one shown in Figure 3.2, can have up to 128 lasers inside. The more lasers, the higher is the resolution of the 3D point cloud built. Billions of points are captured in real-time to create a high-resolution 3D model of the vehicle's surroundings called a "point cloud", scanning the environment up to 300 meters around the car, and within a few centimeters of accuracy. LiDARs are very precise sensors, nevertheless, their ability to perceive the environment can be lowered by interference from rain, fog, smoke and other occlusions in the air. But, since they operate independent of ambient light (they use their own light), they are not affected by shadows, darkness, sunlight or oncoming headlights. LiDAR sensors are usually more expensive than RADAR ones because of their mechanical complexity. LiDARs are used really often in combination with cameras because they cannot detect colors nor can they

read the text as well as cameras. They demand less external processing power, but they are also more expensive than cameras.
The characteristics of LIDAR are:

• Great accuracy on distances and information;
• A higher resolution than the radar sensor;
• 360 degree visibility of the surrounding environment;
• It is expensive.

3.3. Ultrasound Sensors

SONAR (Sound Navigation and Ranging), aka “ultrasound” sensors [7] produce high-frequency audio on the order of 48 kHz. These sensors release an ultrasonic burst and then they listen for the coming back reflections from nearby obstacles. Ultrasound sensors, like the one shown in Figure 3.3, are strongly used in backup detection and self-parking sensors different vehicles. They are mounted on the back, front and corners of cars. Since they work by moving the air and then observing acoustic reflections, they are ideal for low speed uses, when the air around the car is generally not moving very fast. They can be perturbed by wind noise, so they don’t work well at high vehicle speeds. Since they have acoustic nature, performance can be perturbed by exposure to an extremely noisy environment. Ultrasound sensors have a limited range compared to radar sensors, which is why they are not used for measurements requiring high distance, such as automated cruise control or high-speed driving. But if the obstacle is within 2.5 to 4.5 meters of the sensor, it could substitute radar that are more expensive. Since their range is limited, these sensors are not used for navigation and they cannot observe obstacles smaller than 3 cm.

Figure 3.3: SONAR sensor, from [7]

The characteristics of ultrasound sensors are:

• They are inexpensive;
• They can perceive an object few meters away;
• They don’t work correctly at high speeds

3.4. RADAR

In this paragraph the main characteristics of radar sensor, shown in Figure 3.4, are listed briefly for completeness, but since all the thesis turns around it, how radar sensors work is described in deep in the next chapter. In few words it could be said that radar works in the same way of the lidar except for the impulse, instead of light it uses electromagnetic waves belonging to the spectrum of radio waves. It provides the position, distance, velocity and the angle of arrival of an object, by evaluating the time of return of the impulse to the source. Radar can perceive obstacles at a greater distance than other sensors, which is crucial for high-speed driving. They work well in the dark and also when the air is occluded by dust, rain, fog, etc. They can’t build models as precisely as cameras or lidars or detect very small obstacles as other sensors can.

Figure 3.4: RADAR sensor, from [5]

The characteristics of the radar are:

• To guarantee optimum operation in adverse weather conditions;
• Low resolution;
• It is the most used car sensor in the field of obstacles perception;
• It is cheap.

Chapter 4

4. Automotive Radar Systems

RADAR, from “RAdio Detection And Ranging”, is an electronic system able of perceiving the presence of objects in the surrounding environment, commonly called targets, using radio frequency electromagnetic waves [8], [9]. Its operation is based on a physical phenomenon called “Backscattering”, that consists in the dispersion of electromagnetic radiation as a result of the interaction between it and a target larger than the wavelength of the incident radiation.

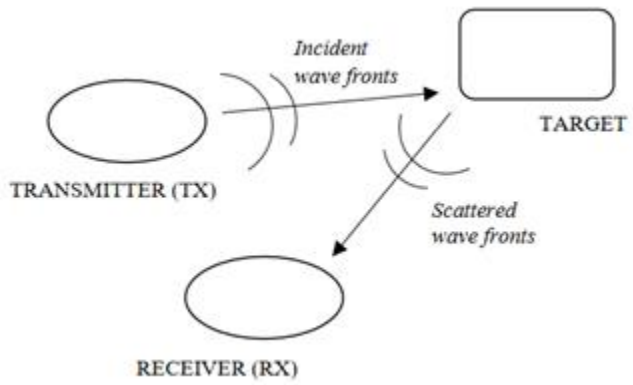

Figure 4.1: Block scheme of a generic radar system, from [8]

The radar system in its simplest configuration is made of two elements: a transmitter and a receiver, as shown in Figure 4.1. The transmitter sends a waveform that hits the target and returns in the form of an "echo" to the receiver, that processing it gets information about the obstacle, for example, about its distance, speed, angle of view and size, depending on the radar type [10], [11]. In particular, the return radiation can be detected by the receiving antenna after a certain delay, equal to twice the target-antenna propagation time. Knowing the speed of propagation of the electromagnetic wave (speed of light) in the considered medium it is thus possible to evaluate the distance of the obstacle and its angular position with respect to the reference system if several antennas are used (radar multiple-input multiple output – MIMO). Considering transmitted signals modulated in frequency it is also possible to compute the speed of moving targets, thanks to the principle of the Doppler effect.

4.1. Fundamentals of radar technology

In a radar system, in general, the signal sent by a transmitter is radiated into the surrounding environment by a transmitting antenna (TX). The electromagnetic wave is then reflected by the obstacle and is processed by the receiver antenna (RX). The received signal is affected by various interference during its path, such as the environmental noise and the noise of electronic components, the electromagnetic interference produced by other signals external to the system, the interference due to reflections on other non-interesting obstacles (clutter) and disturbances due to other electronic devices nearby. The aim of the receiver is thus to identify the signal among the disturbances and then process it. Radar systems can be classified considering the type of the emitted wave: Continuous Wave Radars send continuously signal in the medium, while the Pulsed Wave Radars send finite impulses of short duration, to overcome the problem of overlap between transmitted and received signal. It is possible to make a distinction based also on the configuration of the TX and RX. Typically, the TX and RX are co-located and use the same antenna for both transmission and reception (mono-static radar). In case the TX and RX are separated you have a bi-static or multi-static radar if there are more TX and RX. Multi-static radars are advantageous as they

increase the ability to perceive an obstacle thanks to observation from several points of view. With reference to the case of mono-static radar, the fundamental equation of radar systems gives a relation between the received power and the transmitted power and the distance radar-target. Let P_T be the transmitted power and G_T the transmitting antenna gain, the power density at distance R is:

$$S_T = \frac{P_T G_T}{4\pi R^2} \quad [W/m^2] \qquad (4.1)$$

The power incident on an obstacle at a distance R therefore decreases with the square of the distance between radar and target. The received power density by the radar after a reflection on the obstacle is expressed as:

$$S_R = \frac{P_T G_T}{4\pi R^2} \frac{\sigma}{4\pi R^2} \quad [W/m^2] \qquad (4.2)$$

where σ is called "Radar Cross Section" (RCS) and measures the ability of the target to reflect the incident wave. The higher is the RCS, the greater the possibility that the object is perceived correctly from the radar. The effective A_R area of the receiving antenna is defined as:

$$A_R = \frac{G_R \lambda^2}{4\pi} \quad [m^2] \qquad (4.3)$$

with G_R gain of the receiving antenna and λ the signal's wavelength. To get the received power P_R it is required to multiply the received power density S_R for the effective area A_R of the antenna receiver, obtaining the radar's fundamental equation:

$$P_R = \frac{P_T G_T \sigma G_R \lambda^2}{(4\pi)^3 R^4} \quad [W] \qquad (4.4)$$

Using equation 4.4 is possible to obtain parameters such as P_T or λ knowing the desired minimum P_R value, based on receiver sensitivity. It is necessary to underline that the

received power is inversely proportional to the fourth power of the distance from the target and directly proportional to the square of the wavelength of the signal.

4.2. The Frequency Modulated Continuous Wave Radar

Among the continuous wave radars, very widespread in the automotive industry, there are "frequency modulated continuous wave radar" (FMCW Radar) [12], [13]. These systems are capable to perceive an obstacle and derive different parameters such as speed and distance. The FMCW radar use the "chirp", a sinusoidal signal which frequency increases linearly over time. The signal has a certain bandwidth B, a Tc duration and an initial frequency f_c. Figure 4.2 shows a chirp signal and its amplitude as a function of time.

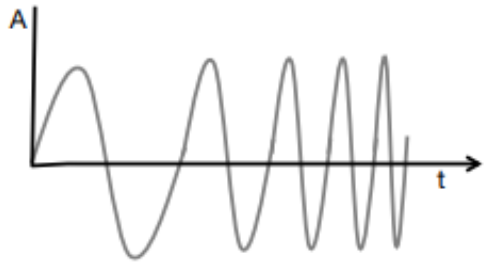

Figure 4.2: Chirp signal with its amplitude as function of time, from [12]

Another way to represent the chirp signal is the one shown in Figure 4.3, where the frequency-time graph illustrates the slope line S that corresponds to the rate of increase of the frequency of the signal and is equal to the ratio between band and signal duration. In the example shown in Figure 4.3, f_c = 77 GHz, B = 4 GHz, Tc = 40 µs and S= 100 MHz/µs.

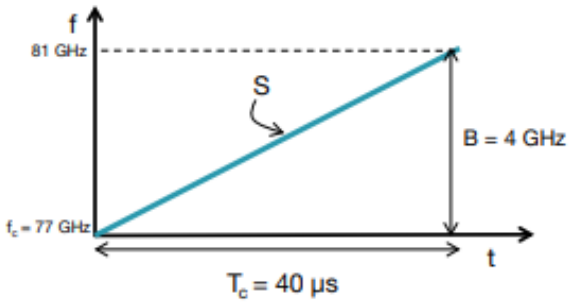

Figure 4.3: Chirp signal with its frequency as function of time, from [12]

Figure 4.4 represents a block diagram of the main RF components of an FMCW radar. The radar works as follows:

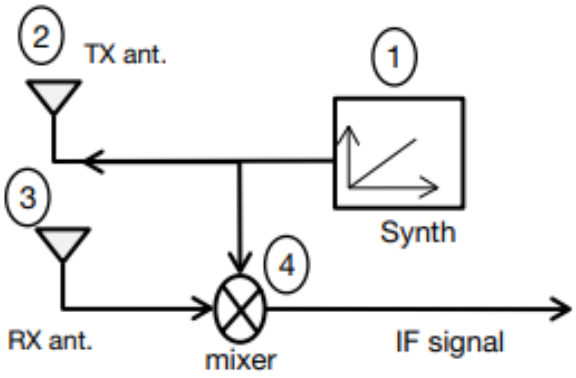

Figure 4.4: FMCW Radar block diagram representation, from [12]

• A synthesizer (synth) creates a chirp signal.

• The chirp signal is transmitted by a transmit antenna (TX ant).

• The reflection of the chirp by a target produces a reflected chirp captured by the receive antenna (RX ant).

• A "mixer" combines the RX and TX chirps to obtain an intermediate frequency (IF) signal.

A frequency mixer is an electronic component that combines two signals to generate a new signal with a new frequency. For two sinusoidal entries x_1 and x_2:

$$x_1 = \sin(\omega_1 t + \phi_1) \qquad (4.5)$$

$$x_2 = \sin(\omega_2 t + \phi_2) \quad (4.6)$$

The output x_{out} has a frequency equal to the difference of the frequencies of the two inputs. The phase of x_{out} is the difference of the phases of the two input signals:

$$x_{out} = \sin[(\omega_1 - \omega_2)t + (\phi_1 - \phi_2)] \quad (4.7)$$

How the mixer works can also be understood graphically by observing at TX and RX chirp frequency representation as a function of time. The upper diagram in Figure 4.5 shows TX and RX chirps as a function of time for a single target perceived. Notice that the RX chirp is time delayed respect the TX chirp. The time delay (τ) can be derived as:

$$\tau = \frac{2d}{c} \quad (4.8)$$

where d is the distance to the target and c is the speed of light. To get a representation of the frequency, as a function of time, of the IF signal at the output of the frequency mixer, subtract the two lines presented in the upper part of Figure 4.5. The distance between the two lines is fixed, which means that the IF signal has a constant frequency. Figure 4.5 shows that this frequency is $S\tau$.

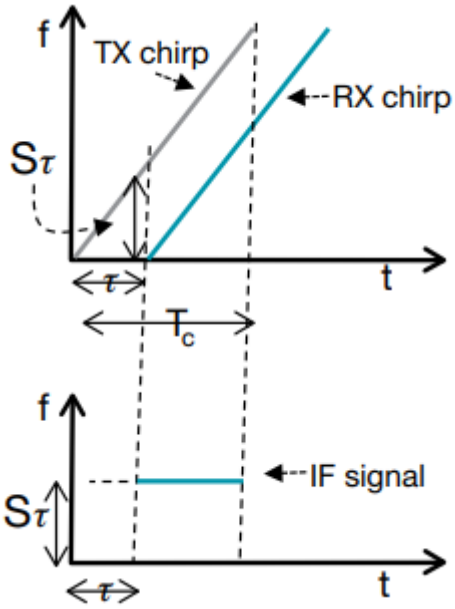

Figure 4.5: IF signal, from [12]

The output of the mixer is a sine wave with a magnitude function of time since it has a constant frequency. The initial phase of the IF signal (ϕ_0) is the phase difference between the TX chirp and the RX chirp at the time instant corresponding to the start of the IF signal (i.e., the time instant represented by the left vertical dotted line in Figure 4.5).

$$\phi_0 = 2\pi f_c \tau \qquad (4.9)$$

It can be further treated obtaining:

$$\phi_0 = \frac{4\pi d}{\lambda} \qquad (4.10)$$

Summarizing, for a target at a distance d, the IF signal will be a sine wave, then:

$$IF = A\sin(2\pi f_0 t + \phi_0) \qquad (4.11)$$

Where:

$$f_0 = \frac{S2d}{c} \qquad (4.12)$$

and equation (4.10) gives ϕ_0.

So by evaluating f_0 you can derive the distance between radar and target inverting the equation.

If there are more objects, the received signal is a composition of different sinusoidal tones. In this case the Fourier transform permits to separate the tones in the frequency domain.

A sinusoid over time is known to produce a single peak in frequencies; in the presence of several superimposed sinusoidal tones (i.e. more target are perceived) generally an observation window temporal Tc is enough to distinguish separate frequency peaks from $\Delta f > \frac{1}{Tc}$ Hz. If the frequencies of the two sinusoids are too much close each other to the considered Tc, they will be displayed as a unique peak.

Figure 4.6 shows three different RX chirps received from different targets. Each chirp is delayed by a different amount of time that is proportional to the distance. The RX chirps translate to multiple IF tones, each of them with a constant frequency.

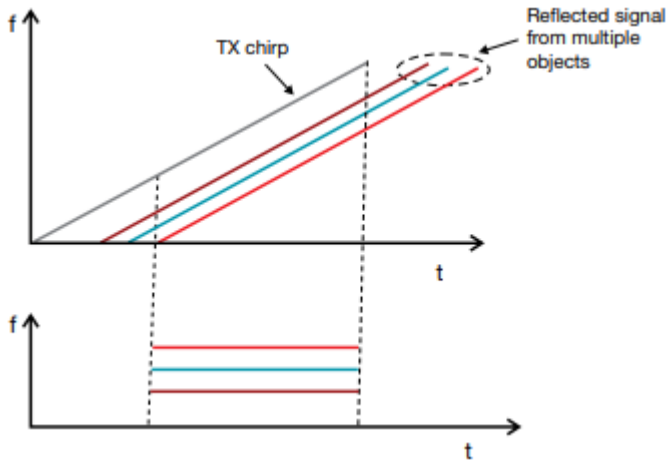

Figure 4.6: Multiple IF signals for multiple object detection, from [12]

This IF signal (consisting of multiple tones) needs to be processed using a Fourier transform in order to isolate the different tones. Fourier transform processing will result in a frequency spectrum that has different peaks for the different tones, each peak indicating the presence of a target at a specific distance.

4.3. Radar range resolution

Range resolution is the capability to distinguish between two or more targets. When two objects move closer, at some point, a radar will no longer be cable to differentiate them as separate [14]. Fourier transform theory affirms that you can improve the resolution by increasing the length of the IF signal. To expand the length of the IF signal, the bandwidth must also be expanded proportionally. An increased length IF signal results in an IF spectrum with two different peaks. Fourier transform theory also says that an observation window (T) can solve frequency components that are differentiated by more than $\frac{1}{T}$ Hz. This means that two IF signal tones are resolved in frequency as long as the frequency difference satisfies the following relationship:

$$\Delta f > \frac{1}{Tc} \qquad (4.13)$$

where Tc is the interval of observation.

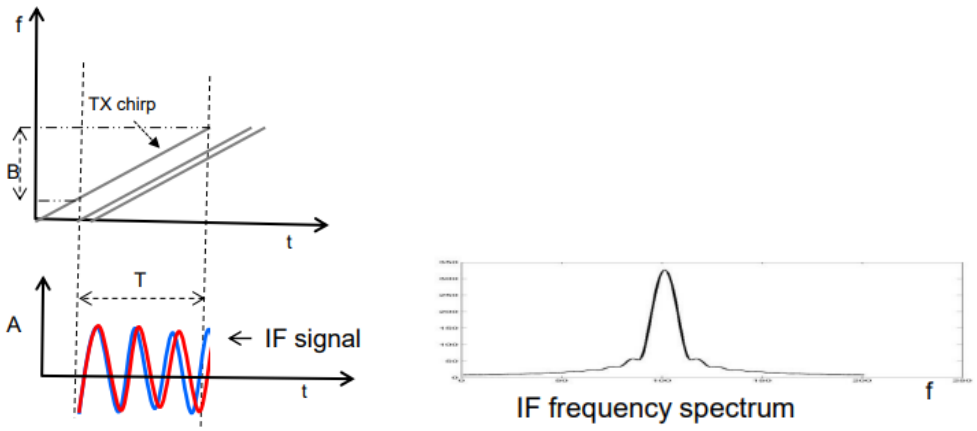

Figure 4.7 : IF signal of two targets too close, from [14]

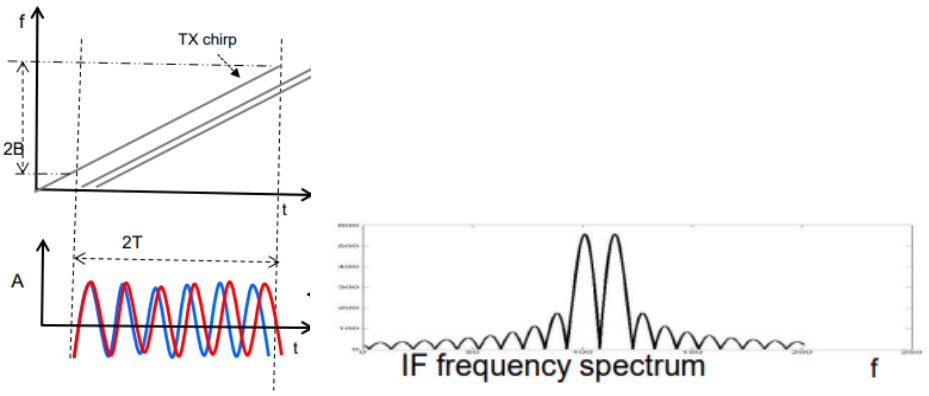

Figure 4.8: IF signal of two targets increasing Bandwidth, from [14]

In Figure 4.7 the two targets are too close that they turn out as a unique peak in the frequency spectrum. The two objects can be distinguished by increasing the length of the IF signal. This proportionally increases the bandwidth as shown in Figure 4.8. Therefore, greater is the Bandwidth better is the range resolution.
Since:

$$\Delta f = \frac{S2\Delta d}{c} \qquad (4.14)$$

and $B = ST_c$, the equation can be written as:

$$\Delta d > \frac{c}{2ST_c} = \frac{c}{2B} \qquad (4.15)$$

The range resolution (d_{Res}) depends only on the bandwidth of the chirp:

$$d_{Res} = \frac{c}{2B} \qquad (4.16)$$

Therefore, a FMCW radar with a chirp bandwidth of a few GHz has a resolution in the order of centimeters (e.g., a chirp bandwidth of 4 GHz corresponds to a resolution of 3.75 cm).

4.4. Phase of the IF signal

If two objects are equidistant from the radar (Figure 4.9) the range-FFT would have a single peak.

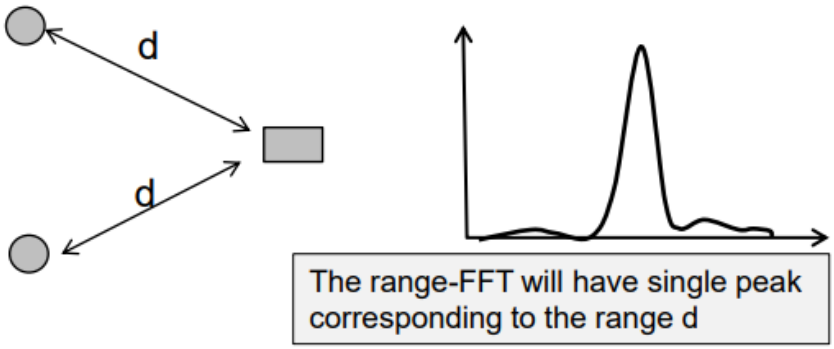

Figure 4.9: FFT of two objects at the same distance from the radar, from [14]

In order to distinguish these two targets if they have different relative velocities to the radar, then they can be separated out by further signal processing. To better understand that we need to look at the phase of the IF-signal. As shown in Figure 4.10 a sinusoid in the time domain generates a peak in the frequency domain. In general, the signal in the frequency domain is complex (i.e. each value is a phasor with a phase and a amplitude).

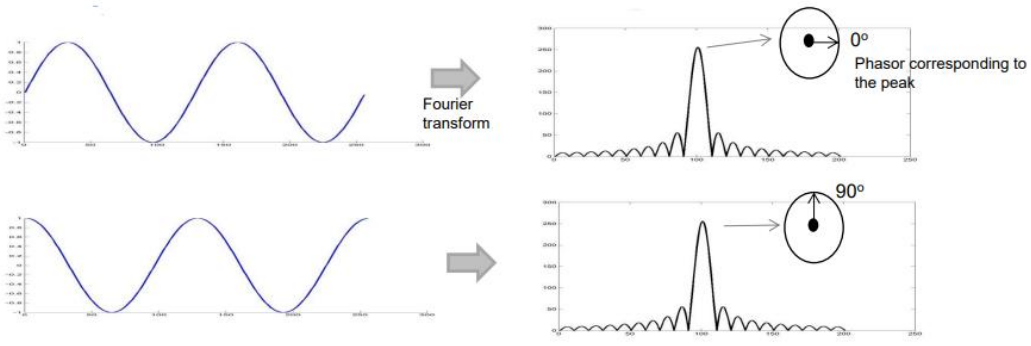

Figure 4.10: Fourier Transform of a sinusoid signal, from [14]

To get more intuition, let's look at the 'A-t' graph and let's observe what happens

changing the round-trip delay by a small amount Δτ. Consider that the initial phase of the signal at the mixer output is the difference of the initial phases of the two entries.

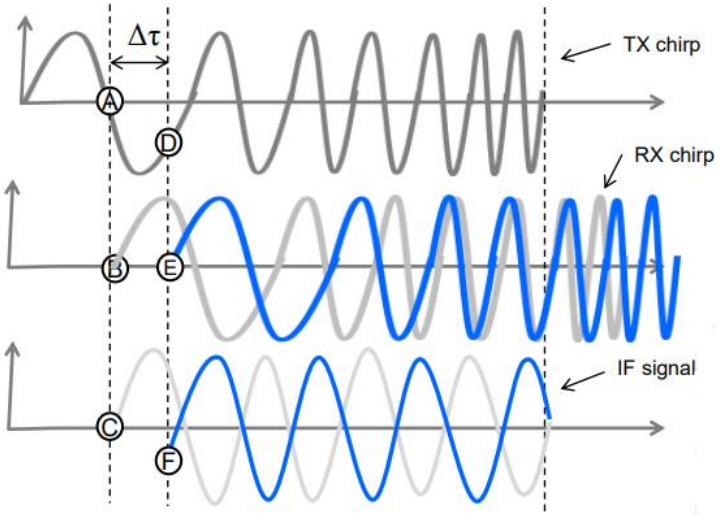

Figure 4.11: Amplitude-Time graphs for TX chirp, RX chirp and IF signal, from [14]

Phase difference between point A and point D is $\Delta\phi = 2\pi fc\Delta\tau = \frac{4\pi\Delta d}{\lambda}$. This is also the phase difference between point C and point F in Figure 4.11.

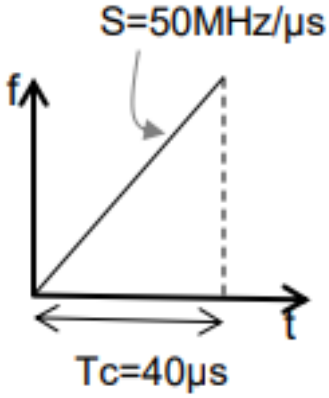

Figure 4.12: Chirp example, from [14]

Consider the chirp shown in Figure 4.12. If a target in front of the radar changes its position by 1mm (for 77GHz radar 1mm= λ /4):

• The phase of the IF signal moves by $\Delta\phi = \frac{4\pi\Delta d}{\lambda} = \pi = 180°$

• The frequency of the IF signal moves by $\Delta f = \frac{S2\Delta d}{c} = 333$ Hz.

Now, 333 Hz looks like a big number, but in the observation window it corresponds to only additional $\Delta f\, T_c = 333x40x10^{-6} = 0.013$ cycles. This changing would not be visible in the frequency spectrum (see Figure 4.13) while the phase of the IF signal is more sensitive to small changes in target range.

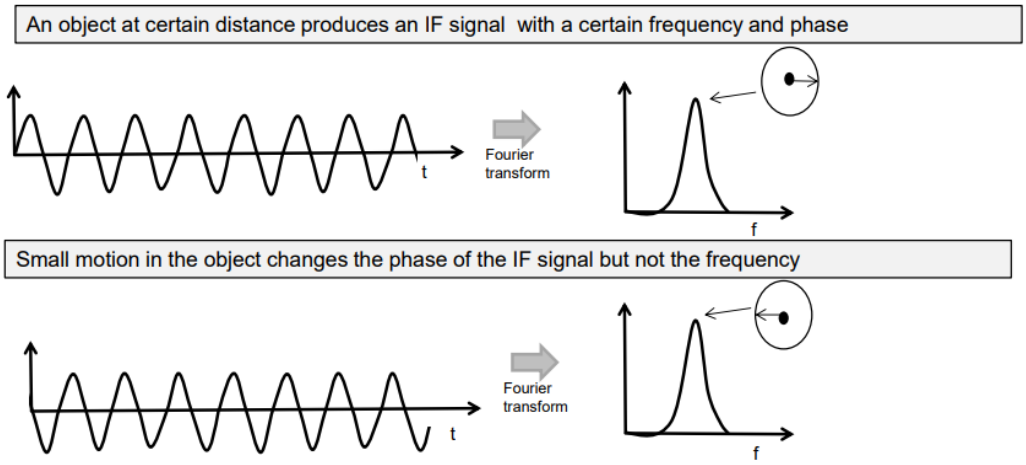

Figure 4.13: Sensitivity of the IF signal to small displacements of the target, from [14]

4.5. Velocity evaluation in FMCW radar

In order to evaluate speed, a FMCW radar transmits two chirps separated by T_c (see Figure 4.14). Each reflected chirp is then processed through FFT to detect the range of the target (range-FFT). The range-FFT corresponding to each chirp will have peaks at the same point, but with a different phase. The evaluated phase difference corresponds to a movement of the target of vT_c.

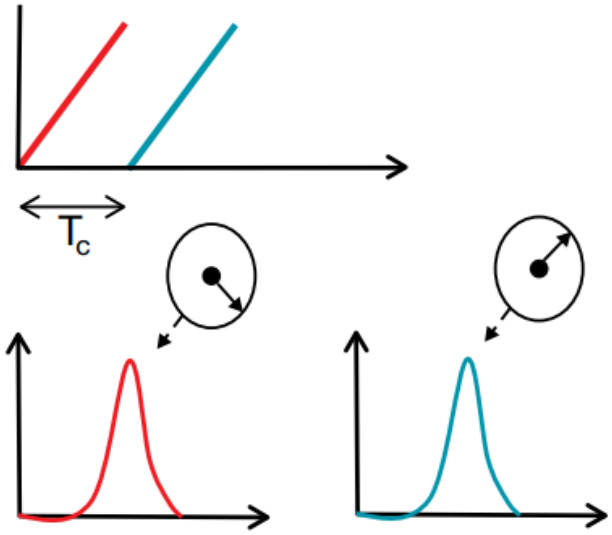

Figure 4.14: Two-chirps velocity measurement, from [12]

The phase difference is derived from equation 4.10 as:

$$\Delta\phi = \frac{4\pi v T_c}{\lambda} \qquad (4.17)$$

The velocity can be derived using equation 4.18:

$$v = \frac{\lambda\Delta\phi}{4\pi T_c} \qquad (4.18)$$

Since the speed measurement is based on a phase difference, there is ambiguity. The measurement is not ambiguous only if $|\Delta\phi| < \pi$.
Using the equation 4.18, it is possible derive:

$$v < \frac{\lambda}{4T_c} \qquad (4.19)$$

the maximum relative speed (V_{max}) that the radar system can detect using two chirps transmitted over a time distance of T_c is then obtained. Higher V_{max} wants shorter transmission times between chirps:

$$V_{max} = \frac{\lambda}{4T_c} \qquad (4.20)$$

4.6. Velocity evaluation with multiple objects at the same range

Examine a discrete signal corresponding to a phasor rotating a constant rate of ω radians per sample. An FFT on these series of samples generates a peak with the location of the peak at ω (see Figure 4.15).

Figure 4.15: FFT of a discrete signal, from [14]

If the signal is the sum of two phasors, as shown in Figure 4.16, the FFT has two peaks (each phasor rotating respectively at the rate of ω_1 and ω_2 radians per sample).

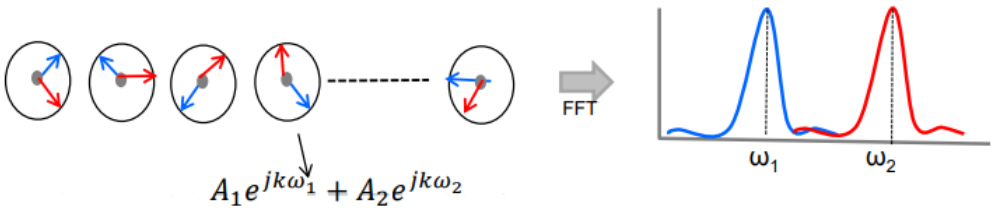

Figure 4.16: FFT of a discrete signal as composition of two distinct phasors, from [14]

• ω_1=0, ω_2=π/N. Over N samples, the 2nd phasor has travel over π rads more than the 1st phasor and is not sufficient to solve the two targets in the frequency domain (see Figure 4.17).

Figure 4.17: FFT of a discrete signal as composition of two distinct phasors separated by π rads, from [14]

• Over 2N samples, the 2nd phasor has travel over 2π rads more than the 1st phasor and so two targets are solved in the frequency domain as shown in Figure 4.18.

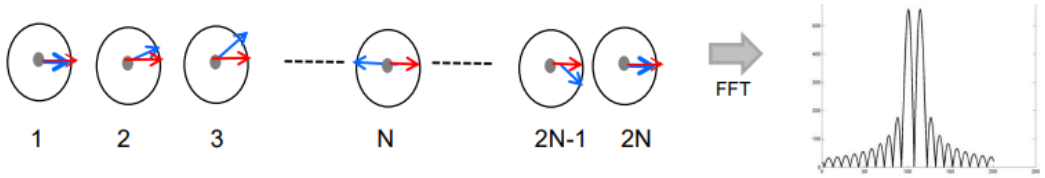

Figure 4.18: FFT of a discrete signal as composition of two distinct phasors separated by 2π rads, from [14]

Longer is the sequence length better is the range resolution. In general, a sequence of length N can differentiate angular frequencies which are separated by more than $2\pi/N$ rad/sample.

Considering the frequency domain resolution criteria for continuous and discrete signals:

• For continuous signals: $\Delta f = 1/T$ cycles/sec;

• For discrete signals: $\Delta\omega = 2\pi/N$ radians/sample $= 1/N$ cycles/sample.

In order to evaluate the speed (v) of a target two chirps separated by T_c are transmitted, the range-FFTs corresponding to each chirp has peaks in the same position but with different phase, the measured phase difference (ω) corresponds to a movement of the object of vT_c.

The two-chirps speed measurement method does not work if multiple moving targets with different speeds are at the time of measurement, both at the same distance from the

radar system. Since these targets are at the same distance, they will generate reflective chirps with the same IF frequencies. As a consequence, the range-FFT results in single peak, that represents the combined signal from all of these equi-range targets. A simple phase comparison technique does not work. In this last case, in order to evaluate the velocity, the radar must transmit more than two chirp signals. It transmits N equally spaced chirps. This set of chirps is named as chirp frame. Figure 4.19 shows the frequency as a function of time for a chirp frame.

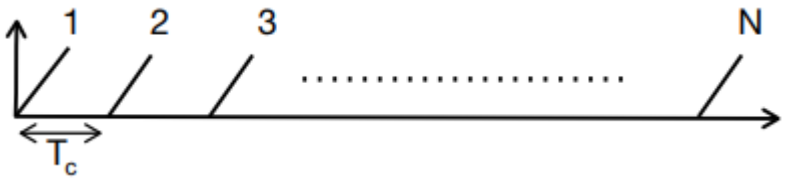

Figure 4.19: Chirp frame, from [12]

Consider for instance two targets equidistant from the radar system approaching it at speeds v_1 and v_2.

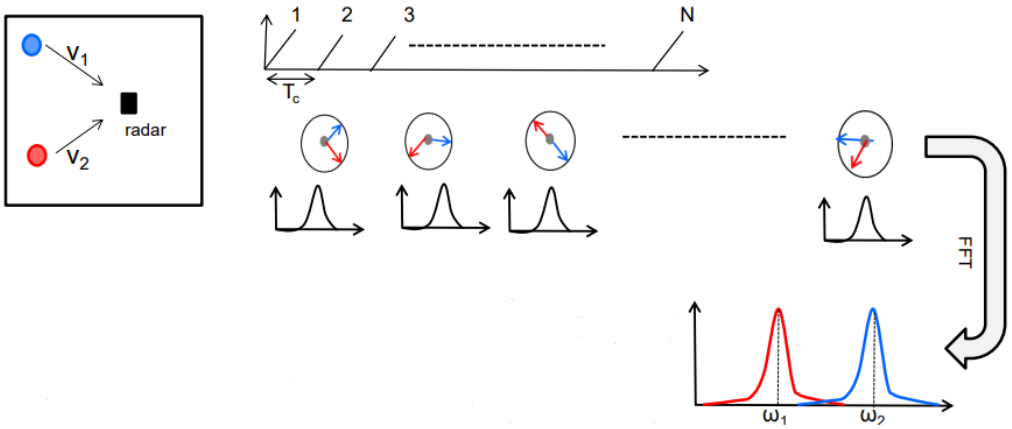

Figure 4.20: Doppler-FFT on the sequence of phasors peaks resolves the two targets, from [14]

A FFT on the sequence of phasors related to the range-FFT peaks solves the two targets. This is called a doppler-FFT (Figure 4.20). ω_1 and ω_2 are related to the phase difference between successive chirps for the respective targets and so the speed of the

two targets can be derived:

$$v_1 = \frac{\lambda\omega_1}{4\pi T_c} \qquad (4.20)$$

$$v_2 = \frac{\lambda\omega_2}{4\pi T_c} \qquad (4.21)$$

4.7. Radar velocity resolution

The theory of discrete Fourier transforms affirms that two discrete frequencies, ω_1 and ω_2, can be solved if:

$$\Delta\omega = \omega_2 - \omega_1 > 2\pi/N \qquad (4.22)$$

Since $\Delta\omega$ is also defined by the equation 4.17, it can be obtained the velocity resolution (v_{res}) if the frame period $Tf = NT_c$:

$$v > v_{res} = \frac{\lambda}{2Tf} \qquad (4.23)$$

The velocity resolution of the radar system is inversely proportional to the frame time (Tf).

4.8. Radar angle estimation

A FMCW radar can evaluate the angle of a reflected signal with the horizontal plane. This angle is also named the angle of arrival (AoA). Angular evaluation is based on the consideration that a small changing in the distance of a target results in a phase change in the peak of the range-FFT or Doppler-FFT. This observation is used to estimate the

AoA, using at least two RX antennas as shown in Figure 4.21. The distance from the target to each of the antennas results in a phase change in the FFT peak. The phase change permits you to estimate the angle of arrival.

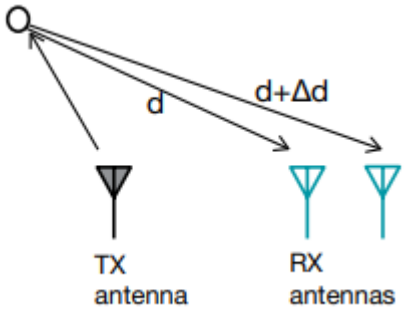

Figure 4.21: Two antennas are required to evaluate AoA, from [12]

In this configuration, the phase changing is got as:

$$\Delta\phi = \frac{2\pi\Delta d}{\lambda} \qquad (4.24)$$

by geometrical reasonings the AoA (θ), can be evaluated from the measured Δϕ with:

$$\theta = \sin^{-1}\left(\frac{\lambda\Delta\phi}{2\pi l}\right) \qquad (4.25)$$

Note that Δϕ depends on sin (θ). This is a nonlinear dependency. sin (θ) is approximated with θ when θ has a small value: sin (θ) ~ θ. As a result, the accuracy depends on angle of arrival and is more precise when θ has a small value (Figure 4.22).

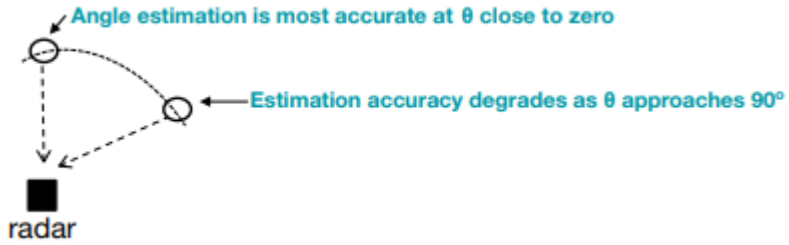

Figure 4.22: AoA measurement is more accurate for small angles, from [12]

The maximum angular field of view (FOV) of the radar system is defined by the maximum angle of arrival that the radar can evaluate. See Figure 4.23.

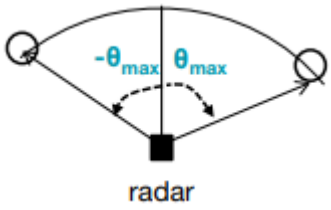

Figure 4.23: Maximum angular field of view, from [12]

Non ambiguous evaluation of angle requires | Δω |< 180°. Using equation 4.25, this corresponds to:

$$\frac{2\pi l \sin(\theta)}{\lambda} < \pi \qquad (4.26)$$

Equation 4.27 shows that the maximum FOV that two antennas spaced l apart can service is:

$$\theta_{max} = \sin^{-1}\left(\frac{\lambda}{2l}\right) \qquad (4.27)$$

A spacing between the antennas of $l = \lambda/2$ results in the largest angular FOV ± 90°. Considering now two targets equidistant from the radar approaching the radar system at the same relative velocity to the radar. The value at the peak has phasor components

from both targets. Hence previous approach does not work. The solution is an array of receive N antennas.

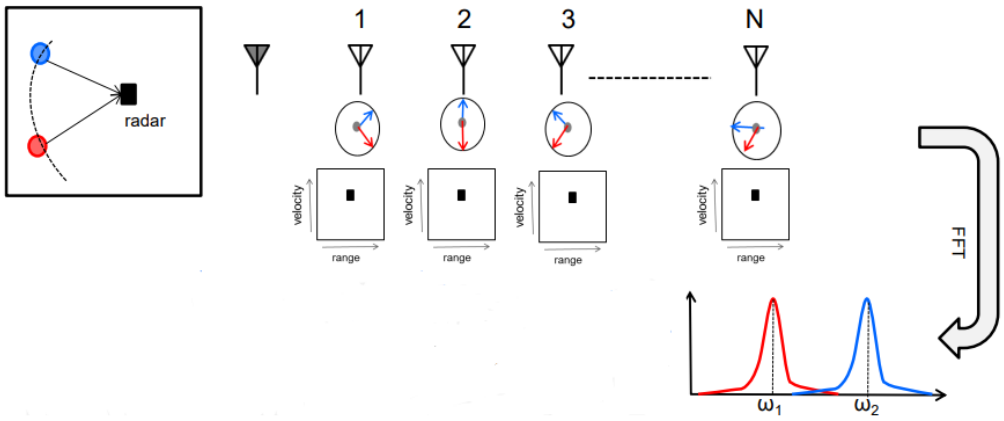

Figure 4.24: Angle-FFT on the sequence of phasors peaks resolves the two targets, from [14]

A FFT on the sequence of phasors corresponding to the 2D-FFT peaks solves the two targets. This is named angle-FFT (Figure 4.24). ω_1 and ω_2 correspond to the phase difference between successive chirps for the respective targets and so the AoA of the two targets can be derived:

$$\theta_1 = \sin^{-1}\left(\frac{\lambda\omega_1}{2\pi d}\right) \qquad (4.28)$$

$$\theta_1 = \sin^{-1}\left(\frac{\lambda\omega_2}{2\pi d}\right) \qquad (4.29)$$

4.9. Radar angle resolution

Angle resolution (θ_{res}) is the minimum angle separation for the two targets so that they are distinguished in the correct way from the radar system and so is the minimum angle separation for the two targets to appear as different peaks in the angle-FFT. It is given by the formula:

$$\theta_{res} = \frac{\lambda}{Ndcos(\theta)} \qquad (4.30)$$

Note that θ_{res} depends on θ (the best resolution is at θ=0).
Resolution is often considered assuming d= λ /2 and θ=0 and so it results:

$$\theta_{res} = \frac{2}{N} \qquad (4.31)$$

The term single-input-multiple-output (SIMO) radar system refers to a radar with a single transmission and multiple receiving antennas. The resolution angle of a SIMO radar depends on the number of RX antennas. For instance, a radar with four RX antennas has an angular resolution of almost 30º, while a device with eight RX antennas has an angular resolution of almost 15º. Thus, in order to improve angular resolution is needed to increase the number of RX antennas. The term multiple-input-multiple-output (MIMO) refers to a radar device with multiple TX antennas and multiple RX antennas. MIMO radars simultaneously radiate not related signals in multiple directions or in one direction only, depending on the configuration. These radars are characterized by better angular resolution and can provide robust interference immunity; in general, the structure provides a set of Nt transmitting antennas and Nr receiving antennas that can observe the target from different angles. In the case of several TX antennas, typically these alternate in transmission while the reflected chirp is received simultaneously by the antennas for RX use.

4.10. Automotive Radar Frequency Bands

Two frequency bands were mainly used for automotive radar systems: the 24 GHz and 77 GHz bands but starting from January 1, 2022, the 24 GHz ultra-wide bandwidth is no more accessible [15], [16]. The relevant frequency bands are shown in Figure 4.25. The 24-GHz band contains an industrial, a scientific and a medical (ISM) band from 24.0 to 24.25 GHz, which is often named the Narrowband (NB), having a bandwidth of 250

MHz. This band is unlicensed. The 24-GHz band also contains an Ultrawide Band (UWB), that is 5 GHz wide. For short-range radar, the 24-GHz NB and UWB bands have been used in legacy automotive sensors. For simple ADAS, like basic BSD, NB ISM could be used, but in most cases, including ultrashort-range radar applications, the need for high-range resolution demanded the use of the UWB band. Due to spectrum regulations and standards established by the European Telecommunications Standards Institute (ETSI) and the Federal Communications Commission (FCC), the ultra-wide bandwidth band has been eliminated. The 24-GHz UWB band is no longer available after January 1, 2022, known as the "sunset date", both in Europe and the USA; only the NB ISM band will be available long term. This absence of wide bandwidth in the 24-GHz band, coupled with the necessity of higher performance in emerging radar applications, makes 24 GHz band not attractive for new radar applications. This is particularly true considering the significant attention in the automotive industry for advanced applications as the automated parking and 360° view. At 77 GHz, there is a 76-77-GHz band accessible for vehicular long-range radar applications. The 77-81-GHz Short- range Radar (SRR) band is a new entry. The availability of wide bandwidth up to 4 GHz in this band makes it of interest for applications requiring high-range resolution. Most 24-GHz automotive radar sensors moved to the 77-GHz band.

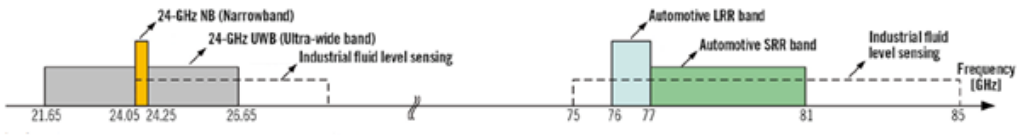

Figure 4.25: 24-GHz and 77-GHz frequency bands, from [15]

Improved range resolution and accuracy

One of the main benefits of 77 GHz band is the wide bandwidth available. Compared to the 200-MHz ISM band, which is accessible at 24 GHz, there is remarkably higher bandwidth available at 77 GHz. In particular, the 77-81-GHz SRR band offers up to 4 GHz of bandwidth. The accessibility of wide bandwidth highly increases range resolution and accuracy. The range resolution of a radar means its ability to separate

two close objects, while the range accuracy means the accuracy in measuring the distance of a single target. Since range resolution and accuracy are inversely proportional to the bandwidth, a 77-GHz radar can achieve 20 times higher performance in range resolution and accuracy respect to 24-GHz radar. The range resolution obtainable is 4 cm (vs 75 cm for 24-GHz radar). High-range resolution results in better separation of targets (such as a person standing close to a vehicle) and guaranties a dense point cloud of detected targets, thus improving environmental modeling and target classification, important for developing ADAS algorithms and enabling autonomous driving features. Also, higher-range resolution helps the radar achieve better minimum distances. For automotive applications like for example parking assist, a minimum distance of perception is very important; the use of 77-81-GHz radar guaranties a significant improvement in this aspect in comparison to devices like ultrasound sensors.

Improved velocity resolution and accuracy

The velocity resolution and accuracy are inversely proportional to the frequency used. Thus, a higher frequency leads to a better velocity resolution and accuracy. Compared to 24-GHz radars, the 77-GHz ones improve velocity resolution and accuracy by factor 3. For automotive park-assist applications for instance, velocity resolution and accuracy are crucial, due to the necessity to accurately maneuver the car at the slow speeds during parking.

Smaller form factor

One of the main improvements of a higher frequency is that the radar size can be smaller. For a desired antenna FOV and gain, the size of the antenna array is about three times smaller each in the X and Y dimensions comparing 77 to 24 GHz band sensors (Figure 4.26).
This size decreasing is considerably useful for automotive applications, where radars need to be set in tight spots behind the bumper, in other spots around the vehicle, including doors and trunks for some proximity applications, and inside the vehicle for

in-cabin applications.

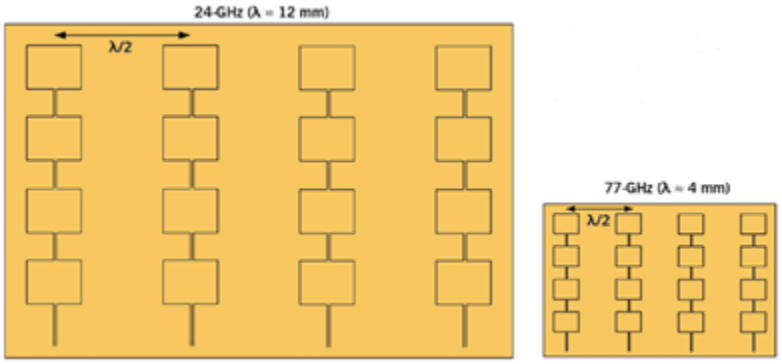

Figure 4.26: 24-GHz and 77-GHz antenna sizes, from [15]

Chapter 5

5. Automotive radar integration and installation

Advanced driver assistance systems (ADAS) have turned up as one of the main areas of research and development in the automotive field. A reason for this has been the push for completely autonomous vehicles. An even more urgent need has been the purpose to make roads safer by equipping vehicles with active and passive safety systems that can help avoid accidents. In order to do that, cars need to be equipped with sensors that map their velocity and position relative to a highly dynamic surrounding environment. Radio detection and ranging (Radar), light detection and ranging (Lidar), optical cameras, and ultrasonic sensors are the most common sensors used. Although they guarantee high-definition images, cameras are costly, need massive computational processing overhead and are perturbed by low visibility conditions. Ultrasonic sensors are cheap and they can be used as proximity sensors for parking, but they have a very restricted detection range of no more than 10 m. Lidar sensors produce high definition 3D images, but they are also costly and are adversely perturbed by car vibrations and inclement weather. Radar has turned up as the main sensor in active safety systems due to its low cost and ability to concurrently detect range, angle of arrival and speed of objects in harsh weather and poor lighting conditions. Nowadays, an increasing quantity of mid- and high-class cars

are equipped with radars providing crucial data for comfort, safety and convenience functions. In the automotive field, sensor placement is an intricate issue that demands consideration of the car body, the performance of the sensor, and the car design. No matter how technically efficient a radar system is, it will not be used in an automotive environment if it does not fit with the design constraints. Often it is necessary to have no interference with the external appearance of the car at all. Automotive radar systems are normally installed behind a plastic and painted bumper or behind other fascia of the vehicle, that means a complicated environment to the sensor and also leads to the degradation of the sensor performance due principally to the reflection on the interface of different media. Before to talk about the integration of the radar into modern cars, it is necessary to underline that the sensor intended as the circuit composed by electronic component such as the transmitters and the receivers, is not installed on the car as it is but is firstly packaged in a plastic cover called radome. The word radome comes from radar and dome, from the shape which characterizes especially the ones used for weather radars [17] as shown in Figure 5.1. A radome is a structural, weatherproof enclosure that protects the radar antennas from weather, dirt and impurities present in the air and conceal antenna electronic equipment from view.

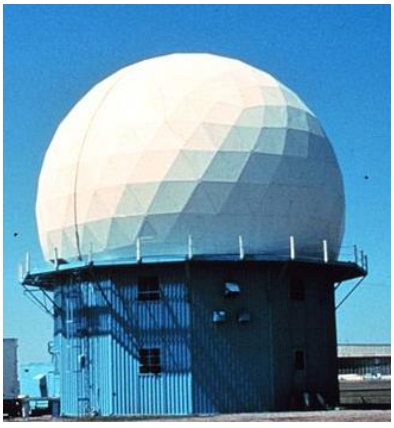

Figure 5.1: Example of weather radar and its radome, from [17]

Radomes used in automotive field have the same aim to protect the radar and maintain the name even if their shapes can vary and could be flat or curved covers. Figure 5.2

shows an example of a possible configuration of the integration of the radar in a car [18].

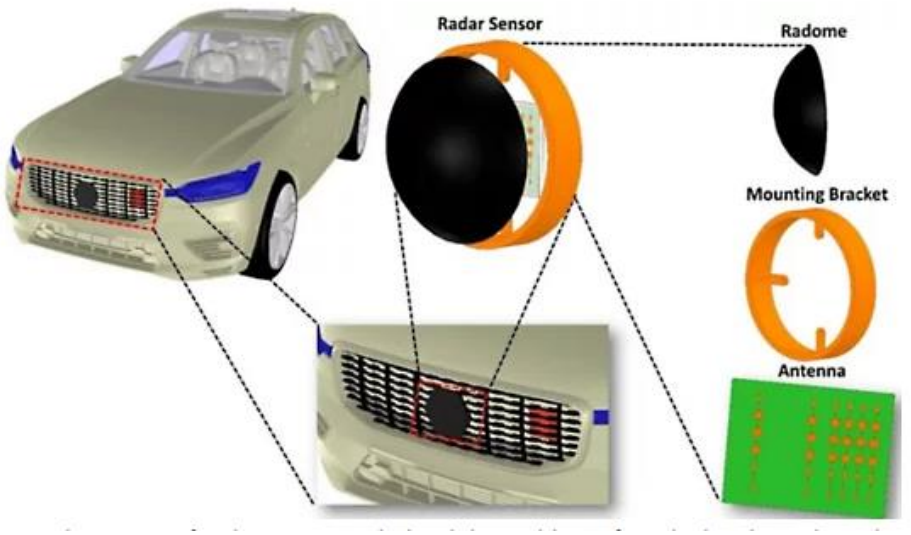

Figure 5.2: Example of the integration of a radar in a car, from [18]

The integration of the radar-radome module can be different and can vary depending on the different constraints of the carmakers (especially from the aesthetic point of view). Figure 5.3 shows five configurations of long-range radar installation corresponding to the most common on the market.

In Figure 5.3a and Figure 5.3b the module is directly mounted on the front of the car, in Figure 5.3c and Figure 5.3d the radome containing the radar is inserted behind a plastic cover (the bumper fascia and air grille respectively), while recently some carmakers put the sensor and its packaging behind the emblem hiding it completely as shown in Figure 5.3e.

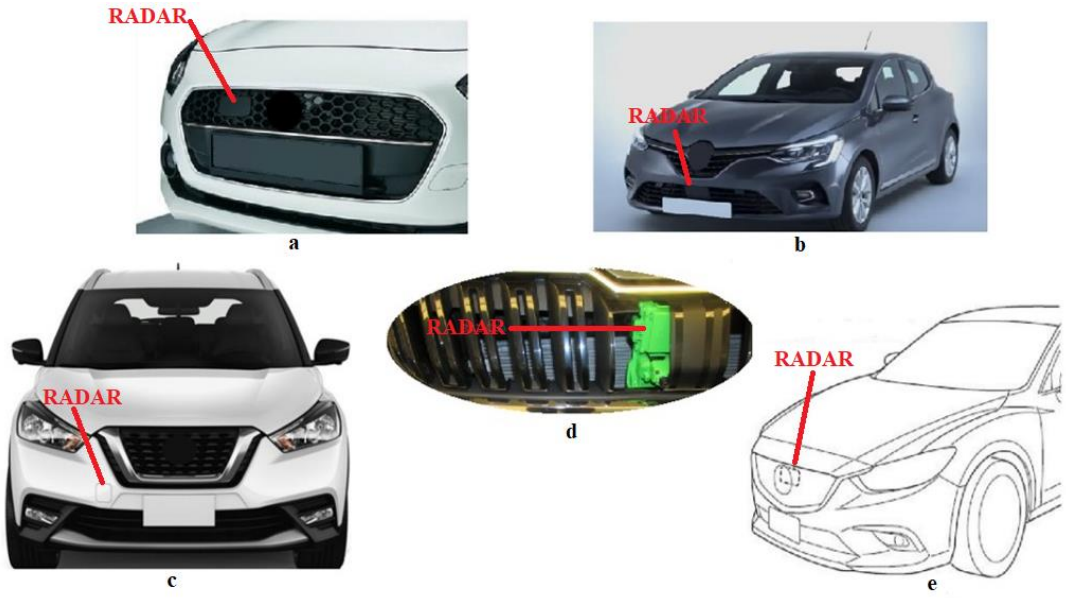

Figure 5.3: Most common configurations of radar module integration used by carmakers

In the most generic case a multi-layers structure [19], [20] is obtained where each layer has to be designed properly in order to not damage too much the radar signals transmission. This structure is shown in Figure 5.4 [21], [22] and the most complex case is the one in which must cope with the degradation of the signal imposed by the radome, by the bumper (or in any case by a layer of plastic such as the emblem or the air grille) and by the different layers of paint with which the outermost surface is treated. For each layer, during the design, different considerations need to be taken regarding material and geometrical features. These considerations are analyzed in the next paragraphs.

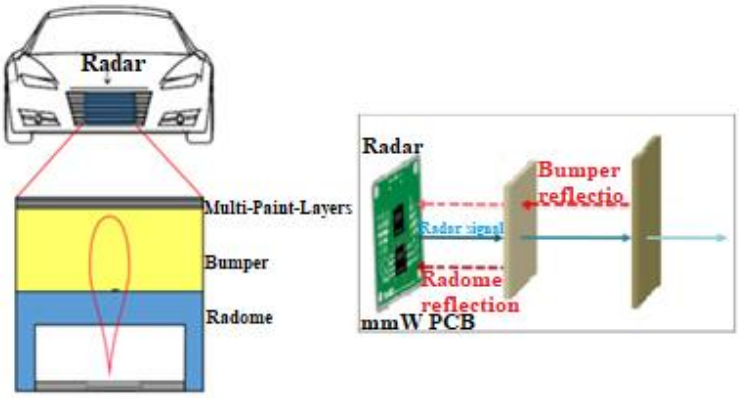

Figure 5.4: Radar installation environment considering multi-paint-layers, bumper and radome, from [21],[22]

5.1. Radar waves propagation through materials

This chapter focuses on electromagnetic (EM) wave propagation through materials [23]. For radars, this is interesting when designing radomes and other layers that radar signals need to pass through. In the procedure of designing a radome, you should always carry out full EM simulation. However, this chapter will help to first evaluate whether a radome can even be functional and how to choose the good materials for the radome and bumper layers.
The first part is a guide on how to describe the radome design in simple words. The physics around EM wave propagation can be hard to understand. This part thus guarantees an overview, with more details in the following paragraphs. Most radome designs procedures are simple, and you can design one so that losses are small enough and will scarcely influence the radar's performance. In the case of a complicated radome design, EM simulations are needed to improve its performance. In these cases, the following considerations can be useful to select the good materials as a starting point in the design.
A radome will always moderately reduce the signal strength of the detected radar objects. Before starting the design procedure, it is thus useful to know the signal-to-noise ratio (SNR) budget. This means that in tests without the radome, you must evaluate how much lower the signal power can be and have the sensor algorithm still working properly. The losses due to the radome must arranged considering this SNR budget. Here there are some general guidelines for the choice of materials:

• Avoid conductors because even small layers produce high attenuation for EM wave propagation;
• Avoid poor dielectrics with elevated loss tangents. Contamination of the radome face might absorb Electromagnetic waves. For instance, a 1 mm water film would determine a high attenuation.
• Ignore materials with high permittivity.

Following these guidelines, it should be doable to correctly design a radome that lead to less than 2 to 3 dB loss. In normal radar system operation, an attenuation of 12 dB will

decrease by fifty per cent the maximum distance of perception. Thus 2 dB will decrease the maximum distance of perception by about 11 percent.

Spacing between the radar and the radome:

• Radomes in the near-field will have an effect on the performance, and a precise study requires electromagnetic simulations.
• Ideally, place the layers at a distance of λ/2 (or multiple of it) from the antennas to reduce the effect of back reflections on the system.
- Distances of λ/4 (or an odd multiple) will have the worst influence on the radar performances.
- This effect is generally weaker than the losses due to reflections. For instance, if the losses due to reflections are in the order of 2 dB, the effect due to the distance is likely below 0.5 dB.
• If the distance between radar and the radome must be minimized at all costs, try to avoid distances smaller than λ/10. There, EM simulations are highly suggested.

Modeling the Field of View (FoV):

• Increasing the FoV will always demands lenses. It is suggested to always simulate the behavior of lenses.
• Decreasing the FoV:
- Sharp edges in the FoV can be obtained with metal's sheets. However, as metal is a strong reflector, EM simulations will have to be carried out.
- Radar beam collimation will always need lenses. It is suggested to always simulate the behavior of lenses.

Vibrations:

• Install the radar rigidly so no vibrations occur.
• Is necessary that no vibrations between the radome and the radar occur.
For EM wave propagation, you must differentiate between reflections on surfaces

(chapter 5.2) and absorption in dielectrics (chapter 5.3). You need to consider the skin effect in conductors (chapter 5.4).

5.2. Reflections on dielectric surfaces

Reflections on dielectric surfaces happen when radar waves must pass through these layers. Snell's law and the Fresnel equations evaluate the behavior of EM waves when they hit these layers. Snell's law states the relationship between incident angle of a ray and the transmitted angle of the ray, as shown in Figure 5.5. The angle of incidence is θi with reference to the normal angle of the surface between two elements. The transmitted ray has an angle of θt to the normal angle.

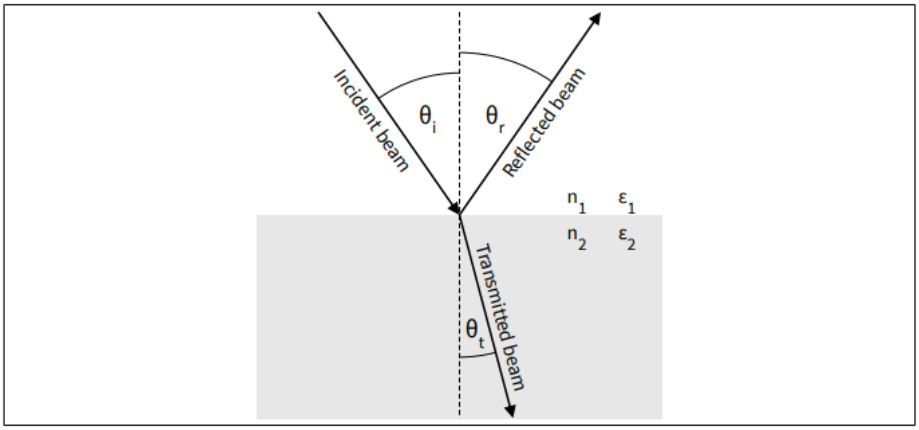

Figure 5.5: Representation of Snell's law, from [23]

The first material has a relative permittivity $\varepsilon_r = \varepsilon_1$, as well as the material on the transmitted side has a relative permittivity $\varepsilon_r = \varepsilon_2$. Since dielectrics are mainly non-magnetic, the refractive index of a material is obtained as the square-root of the relative permittivity:

$$n = \sqrt{\varepsilon_r} \qquad (5.1)$$

The wavelength in the material is obtained as follow:

$$\lambda_{material} = \frac{\lambda_{vacuum}}{n} \qquad (5.2)$$

Snell's law affirms that the product of the refractive index and the sine of the angle are fixed at a surface. Thus, you can write:

$$n_1 \sin(\theta_1) = n_2 \sin(\theta_2) \qquad (5.3)$$

where n_i is the refractive index and θ_i is the ray's angle in the material with relative permittivity ε_i . With that law, you can evaluate the direction of the angle of the transmitted beam with a known incidence angle and known refractive indices (permittivities) at the surface. The crucial fact to remember about Snell's law is that the direction of travel of the beams in a material changes. The shape of the surface of the dielectric material is relevant too. The equations in this chapter consider a flat surface. If you have a curved surface, you need to consider a small section of the surface and approximate it as flat. Generally, a roughness of below one thirtieth of the wavelength can be neglected and treat the surface as flat. In order to evaluate how much of the incident ray is reflected back and how much is transmitted, you will need to consider Fresnel equations. You can differentiate p- from s-polarization: p-polarization is the one parallel to the face. In Figure 5.5, the p-polarization would point from the figure in a third direction. The s-polarization would be normal to the ray's directions in the plane shown in Figure 5.5. All polarizations are superpositions of p- and s-polarization. First, is necessary to assume that the incidence angle is equal to the angle of reflection $\theta_i = \theta_r$.

$$Rp = \left| \frac{n_1 \cos(\theta_t) - n_2 \cos(\theta_i)}{n_1 \cos(\theta_t) + n_2 \cos(\theta_i)} \right|^2 = \left| \frac{n1\sqrt{1-\left(\frac{n_1}{n_2}\sin(\theta_i)\right)^2} - n_2\cos(\theta_i)}{n1\sqrt{1-\left(\frac{n_1}{n_2}\sin(\theta_i)\right)^2} + n_2\cos(\theta_i)} \right|^2 \qquad (5.4)$$

$$R_S = \left| \frac{n_1 \cos(\theta_i) - n_2 \cos(\theta_t)}{n_1 \cos(\theta_i) + n_2 \cos(\theta_t)} \right|^2 = \left| \frac{n_1 \cos(\theta_i) - n_2 \sqrt{1 - \left(\frac{n_1}{n_2} \sin(\theta_i)\right)^2}}{n_1 \cos(\theta_i) + n_2 \sqrt{1 - \left(\frac{n_1}{n_2} \sin(\theta_i)\right)^2}} \right|^2 \quad (5.5)$$

The Snell's law is considered on the first part of the formula to reach the second one. The transmittance T is defined as: T = 1 − R.

Generally, the polarization of the waves sent is not aligned with the face. Thus, the wave sent need to be thought as a superposition of the two different polarizations. Since the two polarizations are transmitted in a different manner, the total polarization of the wave changes when going through a dielectric material.

For an angle of 0 degrees (perpendicular angle to surface), the formulas for both polarizations simplify to:

$$R = \left| \frac{n1 - n2}{n1 + n2} \right|^2 \quad (5.6)$$

5.3. Absorption in dielectrics with loss

In chapter 5.2, it was assumed that the dielectric material of the considered layer was without loss. However, this is not always true. Dielectrics with loss can significantly lower the radio frequency fields passing through them. Figure 5.6 shows how radiation is attenuated in a dielectric with loss.

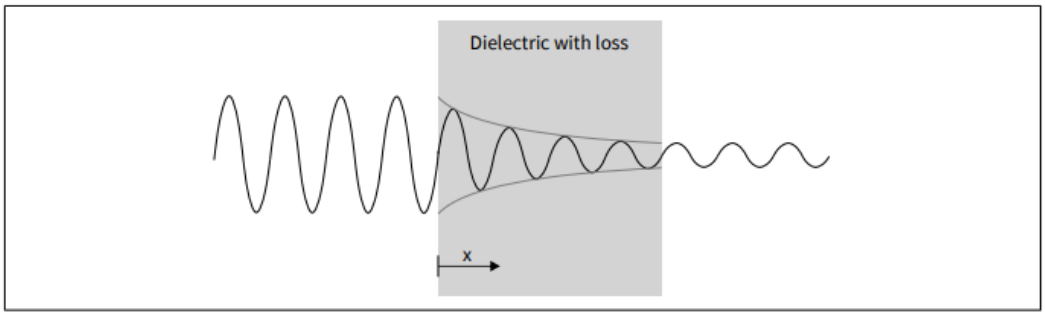

Figure 5.6: Representation of absorption in a material, from [23]

The radiation's power decreases exponentially over material length. To evaluate dielectric loss, a complex permittivity could be used in Maxwell's equations:

$$\varepsilon = \varepsilon' - j\varepsilon'' \qquad (5.7)$$

A different way to think dielectric loss, is by considering the loss tangent as defined as the angle of the complex permittivity in the complex plane:

$$\tan\delta = \frac{\varepsilon''}{\varepsilon'} \qquad (5.8)$$

If the material is also conducting, the loss tangent becomes:

$$\tan\delta = \frac{\omega\varepsilon'' + \sigma}{\omega\varepsilon'} \qquad (5.9)$$

Considering ω as the angular frequency and σ as conductivity. The loss tangent is a property of different material. To compute the losses along the x direction the following formula can be used:

$$P(x) = P(x = 0)\ e^{-\delta\kappa x} \qquad (5.10)$$

With δ= arctan (tanδ) and k is the wavenumber. The wavenumber is obtained from:

$$k = \frac{2\pi}{\lambda} = \frac{2\pi f}{c_0} \qquad (5.11)$$

Where f is the frequency, λ is the wavelength, and c_0 is the speed of light. With these simple formulas and a known loss tangent, is possible to evaluate the absorbed power in the material. In normal radar operation, radar wave have to pass through the material two times, and the losses will be twice as high. The higher is δ, the higher the losses due to absorption will be.

5.4. Skin effect in conductors

If a conductor is present between the radar and the target, you will need to consider skin effect to compute the losses due to the conductor. Like the absorption in a dielectric with loss, skin effect determines an exponential deterioration over the material length. Figure 5.7 shows how radiation is attenuated when a conductor is present. The magnetic field strength of the radiation deteriorates exponentially over material length.

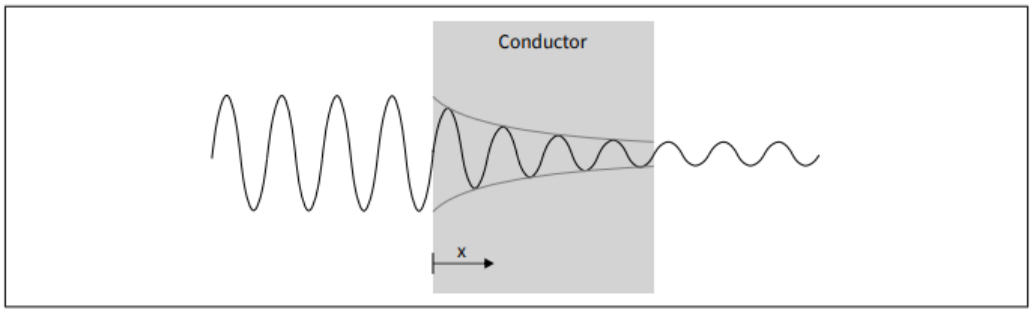

Figure 5.7: Representation of signal attenuation due to skin effect, from [23]

The radiation power depends on the squared magnetic field strength. The magnetic field strength is function of the distance in the conductor:

$$H(x) = H(x = 0)\ e^{-\frac{x}{\delta}} \qquad (5.12)$$

The electromagnetic power is function of the distance in the conductor as well:

$$P(x) = P(x = 0)\ e^{\frac{2x}{\delta}} \qquad (5.13)$$

with the skin depth:

$$\delta = \sqrt{\frac{2\rho}{\omega\mu}} = \sqrt{\frac{2}{2\pi f\sigma\mu_0\mu_r}} \qquad (5.14)$$

Considering σ as specific conductivity, ρ as specific resistivity, μ as the magnetic permeability, f as the frequency and ω as the angular frequency. With these formulas, you can evaluate the power transmitted through a conductor material. Even a thin layer of 1 μm leads to cosiderable reduction of the transmission. Thus, even metal foils (more than 10 μm thickness) will destroy any radar operation through them.

5.5. Far-field and near-field scenarios

It is needed to differentiate between far-field and near-field scenarios. In the far-field, the material is enough far away from the device in such a way there is not any feedback on the antenna behavior. In the near-field instead, it is needed to evaluate these feedbacks.

Far-field scenario

In a far-field application radar's wave has to pass through surfaces like walls or windows. Since buildings can not be modified so easily, it is not always possible to influence the behavior in these applications. But in a well-known environment, you can evaluate the expected losses due to windows or walls to consider the feasibility of a radar sensor use case. In a far-field application, you need to follow only the general considerations.

Near-field scenario

The near-field scenario is suitable if:

$$\text{Distance to antenna} < \frac{2D^2}{\lambda} \qquad (5.15)$$

where λ is the wavelength and D is the maximum linear dimension of the radar antenna.

If the material is placed in the near-field of a radar, it will influence the antenna. This will influence the antenna impedance, which will influence the transmitted and received power. For a detailed analysis of a radome behavior, always carry out full EM-field simulations of the whole system in order to optimize the radar systems behavior. Nevertheless, the next part gives more tips for what to do and what to avoid to do during the procedure of radome design, considerably accelerating it.

5.6. Radomes design guidelines

A radome is a radar enclosure or cover. These covers are generally mounted in the near-field of the radar. When designing radomes, you will need to consider some general reasonings in addition to those listed previously, that are summarized here before.

Reflections on dielectrics

In order to minimize the reflections, a dielectric with low permittivity need to be selected. Moreover, radome materials with low reflections feed back very little to the radar. Fewer reflections from the material layer lower the effect of the radome on the whole radar system.
In a more complete evaluation, even the precise displacement between the antennas and the radome layer matters. If possible, any layer resulting in direct back reflections to the radar sensor should be put with a spacing of λ /2 (or a multiple), as can be seen in Figure 5.8.

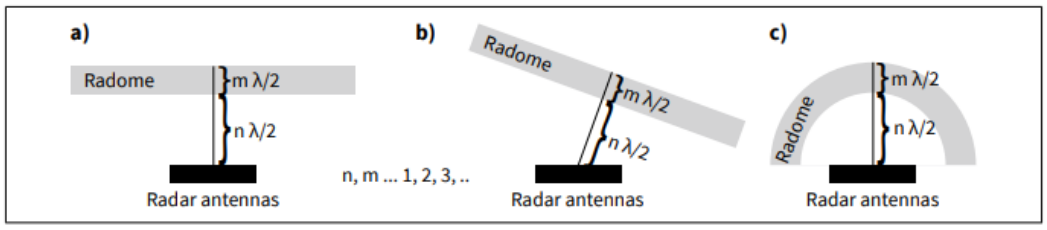

Figure 5.8: Radome dimensioning and spacing from antennas influence back reflections, from [23]

The motivation is that in these conditions, the radar wave travels λ (or even a multiple) to get from the radar transmitter to the radome face that is responsible of the back reflection, and then back to the radar. At this point, the back reflection would be in phase with the new emission. This design minimizes the effect of the back reflections. On the contrary, if the distance is λ /4 (or an odd multiple), the back reflections will be out of phase, and the effect of the back reflections will be maximized. Spherical radomes with the radar antennas in the center (Figure 5.8c) cause back reflections from all possible angles, and thus the effect of the back reflections will be stronger there.

Note: As mentioned in chapter 5.2, the wavelength in a material is lowered by the refractive index.

Note: The power of the signal received will be higher for a radome with low permittivity at the wrong position than a radome with high permittivity at the good position. Back reflections are a secondary aspect to be considered with respect to the material property.

Absorption in dielectrics

Absorption in dielectrics is a phenomenon that increases exponentially over the material length. The material parameter describing the absorption is the loss tangent, that depends on frequency. The loss tangent need to be as low as possible to attenuate absorption. Moreover, when designing a radome, consider if it is possible or not that a water film (or other contamination) could cover the radome.

Conductors

In general, you have to avoid using any conductors in the radomes. Even thin layers of less than 1 μm can result in strong attenuations that destroy radar detection.

Note: Even thin layers of paint with metallic particles could considerably lower the strengths of radar signals.

Curved surfaces and lenses

Curved radomes can lead to different lensing effects. The examples presented give an insight into how to design curved radomes. Figure 5.8c shows the first example of a curved layer. There, the radome is circular, and the radar antennas are set in the center; both surfaces are concentric. The radio frequency waves always hit the radome with an inclination of 90°. Thus, there is no lensing effect and no diffraction (since sin 0° = 0 in equation 5.3). However, all surfaces reflect the signal back to the radar, which impact on the antennas itself. In this case, the back reflections are considerable and it is relevant that the distances of the layers are multiples of λ/2.
Figure 5.9a shows a similar example. The radome is spherical or circular, with both faces concentric. The sensor is shifted away from the concentric center along the optical axis. The resulting beams are deviated when entering and leaving the material. The outgoing and incoming beams are almost parallel but spatially shifted. The result is that there is almost no lensing effect in this implementation. In certain configurations, lenses can be very useful. An instance is an application that demands a narrow-collimated beam in order to perceive an object across a great distance.

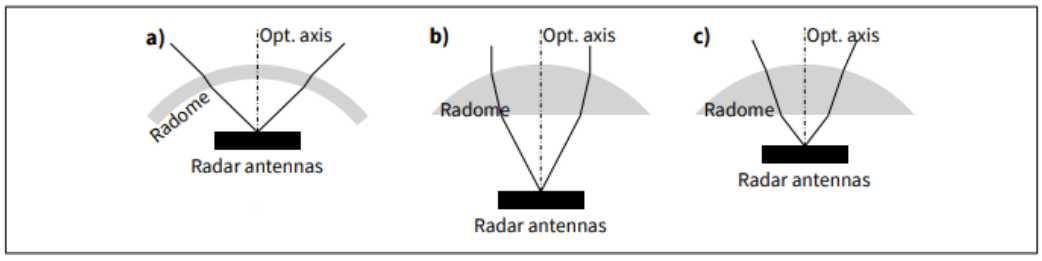

Figure 5.9: Three radomes with curved surfaces, and their effects on beams of radar radiation, from [23]

Note: The incoming beams direction is changed by lenses. Thus, it is suggested to only use lenses when angle estimation is not demanded.

Figure 5.9b shows a radome that acts as a lens. One surface is curved with radius r_1 and the second surface has a curvature with radius r_2 . (In the case of Figure 5.9b, one surface is flat. r_2 -> ∞). The antennas of the sensor are set in the focal point of the lens. After the lens the ray is then collimated. In the collimated ray, the power remains constant during its propagation. In these systems, the target's receiving power diminishes with the second power and not with the fourth power, that improves the maximum distance from which the sensor can perceive an obstacle. To evaluate the focal length f of a thin lens, the following formula can be used:

$$\frac{1}{f} = \frac{n_{lens} - n_{air}}{n_{air}} \left(\frac{1}{r_1} - \frac{1}{r_2} \right) \qquad (5.16)$$

In Figure 5.9c a similar example is shown. The radome is a lens in this case and the sensor is shifted away from the focal point along the optical axis. If the displacement between the radar and the lens is lower than the focal length, the outgoing ray will diverge. On the contrary, the outgoing ray will converge into a single point, which is described by equation 5.17, if the distance between the radar and the lens is higher than the focal length:

$$\frac{1}{a} + \frac{1}{b} = \frac{1}{f} \qquad (5.17)$$

where a is the gap from the radar to the lens and b is the gap from the lens to the converged point.

Note: Things are much more complicated when the radar is not set along the optical axis. Aberrations will occur, and it is suggested to perform a detailed optical analysis.

Vibrations

Vibrations in the radome layer are generally unwanted. The effect of a vibrating radome is discussed in this paragraph. Typically, radomes are close to the radar antennas and reflect a portion of the emitted radio frequency back to the antennas. Vibrations of the radome with respect to the radar change the phase of the reflection. Vibrations at low frequencies are generally not a big obstacle. Nevertheless, if this frequency is in the frequency band of the considered radar signal frequency, the vibrating radome could be perceived as a ghost target in the sensor spectrum at the frequency of vibration.

Note: It is necessary to reduce as much as possible the vibrations of the radome with respect to the sensor. Radar modules need to be installed rigidly to casings that surround them.

Chapter 6

6. Analysis and simulations on the material properties of the multi-layers structure

As discussed in the previous chapters, a radar that is integrated for long-range detection aims in the front of the car, can be installed in different configurations, having in the most general case a multi-layers structure (radome-bumper-coating). A proper design of each of these layers have to be done in order to allow the radar a correct operation.
In this chapter simulations and analysis are done in order to understand what are the materials that can be used for the covers and how the radar signals are attenuated passing through them.
Radomes and bumpers are generally made using plastic materials, simulations about how they reflect and absorb power from electromagnetic waveforms are provided.

6.1. Reflection on plastic surfaces

The most used materials for radomes are polypropylene (PP) and polycarbonate (PC), while bumpers are produced in PP, PC and Acrylonitrile butadiene styrene (ABS), even if as will be showed ABS is not a good choice for the bumper area which has to eventually cover the radar module.
In this section simulations about the reflection (considering an angle of incidence of 0°) of electromagnetic waveforms are done considering these three different plastic materials. Using equation 5.6, it is possible to derive the two different reflection gains, the first one R_1 is get using n_1=n(air) and n_2=n(material) and it gives a result about how much power is reflected back when passing from air to the material of a layer, the second one R_2 is the opposite case (n_1=n(material), n_2=n(air)) and says how much power is reflected back when a radar waveform is leaving the layer towards air.
In Table 6.1 the relative permittivity ε and the corresponding refraction index n of the materials are listed.

	ε	n
Air	1	1
PP	2.2	1.483
PC	2.6	1.613
ABS	2.9	1.703

Table 6.1: Relative permittivity ε and refraction index n for different materials

A transmission gain can be obtained considering T=(1-R_1)*(1-R_2) and it represent how much power is transmitted forward in a single pass transmission. Since in a normal radar operation a double pass transmission is needed, it is better to evaluate T^2, that can be expressed in percentage or in dB for understanding the amount of power that is transmitted. Results are listed in Table 6.2 and shown in Figure 6.1.

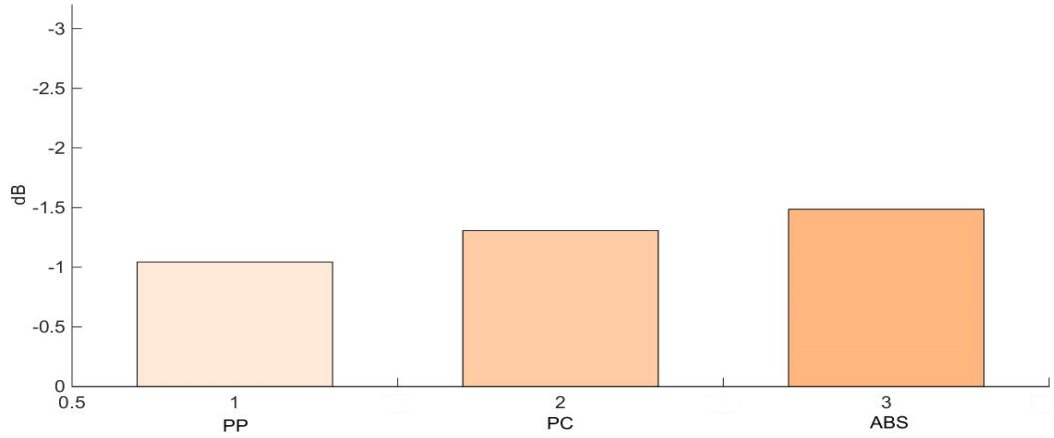

Figure 6.1: Power attenuation due to reflections in different materials

Air – material – air double pass transmission	In %	In dB
PP	78.6	-1.04
PC	74	-1.31
ABS	71	-1.49

Table 6.2: Air-material-air double pass transmission (reflection)

The results show that the three materials have a similar response to reflection phenomenon, but polypropylene is the one causes less attenuation.

6.2. Absorption through plastic surfaces

In this section simulations about the absorption of electromagnetic waveforms are done considering PP, PC and ABS. The first simulation considers a layer of 1 mm width, while the followings consider the typical dimensions of radomes and bumpers, using equation 5.10.

The wave number k depends on the wavelength λ and so on the frequency f that is assumed equal to 77 GHz as the middle one used for long-range detection radars. Table 6.3 shows the wavelength, the wave number and the loss tangent for the material tested.

	λ (in mm)	k (in mm)	δ
PP	2.6	2.4	0.0001
PC	2.4	2.6	0.01
ABS	2.3	2.7	0.02

Table 6.3: Material's wavelength, wave number and loss tangent

Also in this case as for the reflection, a double pass transmission is needed and $P(x)^2$ is so evaluated that can be expressed percentage or in dB for understanding the amount of power that is transmitted. Results are listed in Table 6.4 and shown in Figure 6.2.

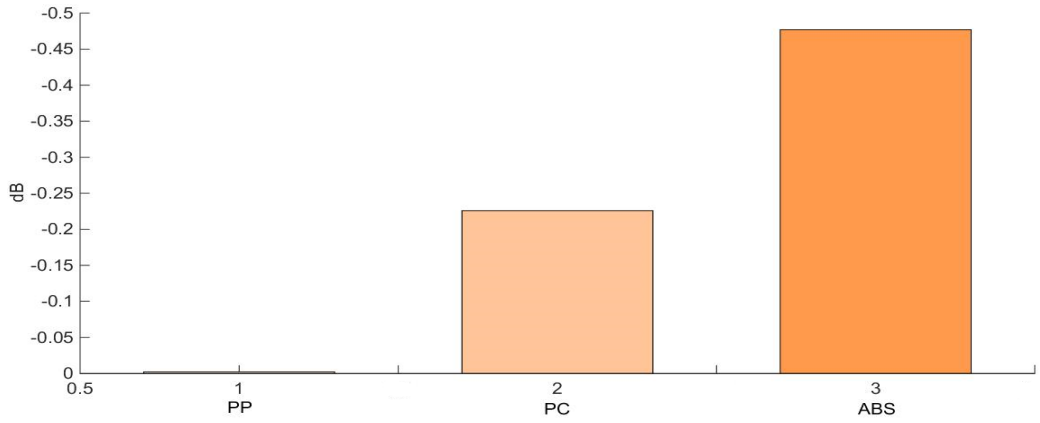

Figure 6.2: Power attenuation due to absorption in 1 mm layer

Air-material-air double pass transmission	In %	In dB
PP	99	-0.002
PC	95	-0.226
ABS	90	-0.477

Table 6.4: Air-material-air double pass transmission (absorption)

Since absorption increases with the width of the considered layers, is useful repeat the simulation considering the dimensions of radomes and bumpers that are commonly around 3 mm and 10 mm respectively. In order to have a proper design we need to consider also some geometric aspects like the one presented in the previous chapter in which to obtain a constructive interference between emitted signals and back

reflections, the spacing between layers and the width of them have to be proportional to a multiple of λ/2. These aspects will be considered later on but now, since we want an equal comparison between materials we will consider a width of 3.6 mm (three times λ (PC)/2) for radome and 10.8 mm (nine times λ(PC)/2) for bumper.
Radome absorption results are listed in Table 6.5 and shown in Figure 6.3 while bumper results in Table 6.6 and Figure 6.4.

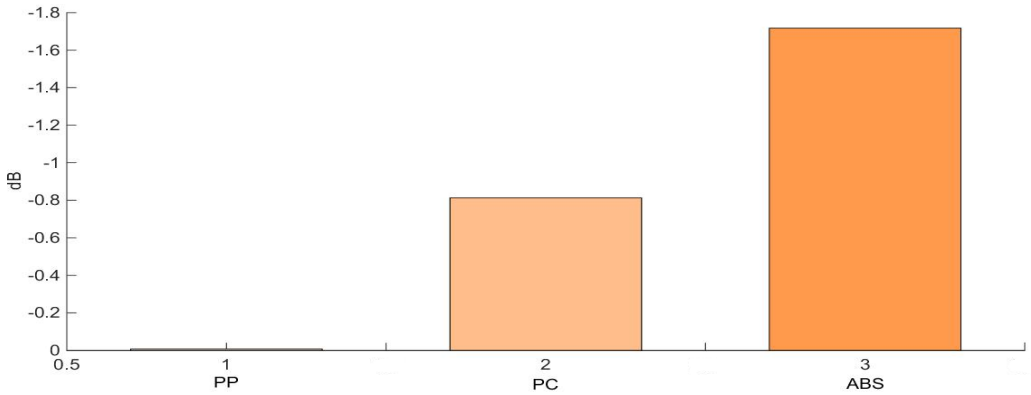

Figure 6.3: Power attenuation due to radome absorption

Air-material-air double pass transmission	In %	In dB
PP	99.8	-0.008
PC	82.9	-0.813
ABS	67.3	-1.717

Table 6.5: Air-material-air double pass transmission (radome absorption)

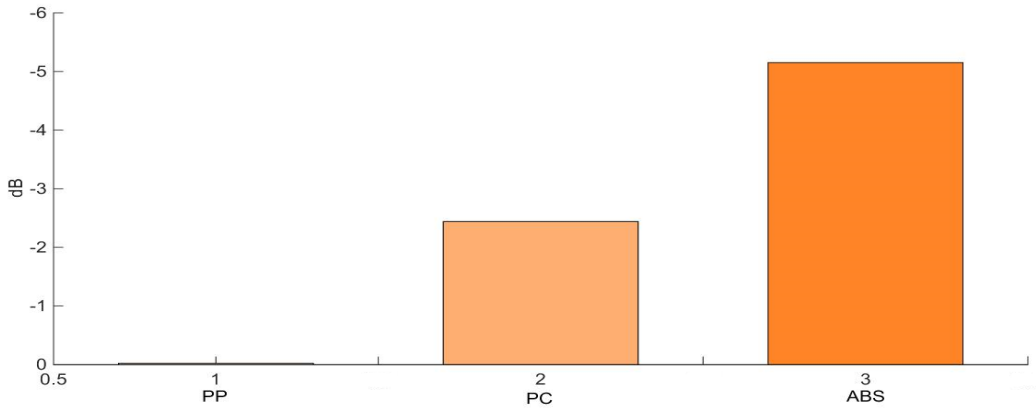

Figure 6.4: Power attenuation due to Bumper absorption

Air-material-air double pass transmission	In %	In dB
PP	99.4	-0.022
PC	57	-2.439
ABS	30.5	-5.152

Table 6.6: Air-material-air double pass transmission (bumper absorption)

Differently to the reflection phenomenon in which similar results are obtained changing the materials, in the absorption case the choice of one of the three different materials considered really matters. In particular, PP has a very low loss tangent that bring it to have a negligible absorption even increasing the width of the layers. Polypropylene results the best plastic and allows to design bumper with higher thickness if required. On the contrary absorption is no more negligible if PC or ABS are used. The power attenuation in a PC radome layer is also in this case not a big obstacle and the results confirm why PC is also very often used for radome design (even if PP ones result better for electromagnetic wave propagation). Even the attenuation of the signal by a PC made bumper do not bring to an interruption of the transmission since a power loss of -2.439 dB is acceptable, but in this case much more attention on the thickness of the bumper need to be made and it must not exceed too much the 10 mm thickness (is preferable stay below the -3 dB attenuation). ABS is often used for bumpers but not in the area of a radome nor for radome itself and simulations confirm that power losses are too much higher.

6.3. Skin effect in conductors and attenuation due to coating layers

The effect of the coating layers of the surfaces above the radar are not negligible as their thickness would suggest. Painting has negligible dimension compared to the other layers (μm of thickness) but it could have metallic components in its composition which could completely destroy the radar transmission. In this paragraph analysis on the power attenuation through 1 μm layer of different metals are done, considering the conductors

that can be more present in automotive paints such as magnesium, aluminum, copper and silver. As written previously the electromagnetic power in this case can be expressed as written into equation 5.13.
The skin depth δ depends on the frequency, the material conductivity and magnetic permeability. Table 6.7 shows the skin depth of the considered materials.

	δ (nm)
Magnesium	229
Aluminum	235
Copper	295
Silver	381

Table 6.7: Skin depth

The double pass transmission $P(x)^2$ is evaluated. Results are listed in Table 6.8 and shown in Figure 6.5.

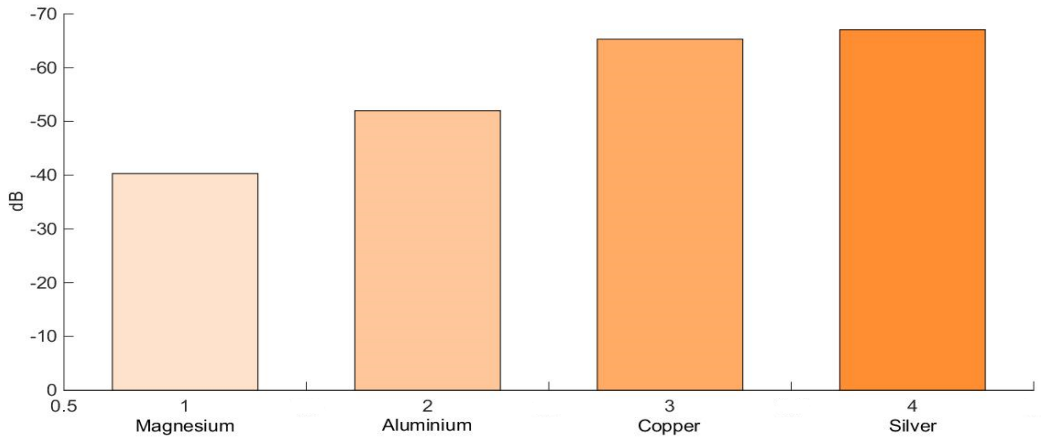

Figure 6.5: Power attenuation due to conductors skin effect

Air-material-air double pass transmission	In dB
Magnesium	-40.3
Aluminum	-52
Copper	-65.3
Silver	-67.1

Table 6.8: Air-material-air double pass transmission (skin effect)

The results show that even a 1 µm layer of metal completely destroy the transmission of

radar signals. If painting is needed it has to be without or with very small (even less of 1%) percentage of metals in its weight. Similar considerations can be done with a thin layer (fraction of mm) of water over the radar covers. This shows why an optimal solution can be install the radar module behind the air grid in such a way a deposit of water is more difficult to appear.

6.4. Power attenuation from radar to environment

In order to simulate the total power attenuation from radar to outside, passing through radome and bumper layers, not only the material properties have to be considered but, as said before, also geometrical aspects that influence the signal transmission. Even if attenuations due to reflection and absorption and so to the material characteristics are the dominant ones, back reflections need to be considered as well.
To do that a Simulink model is provided and it is shown in Figure 6.6.

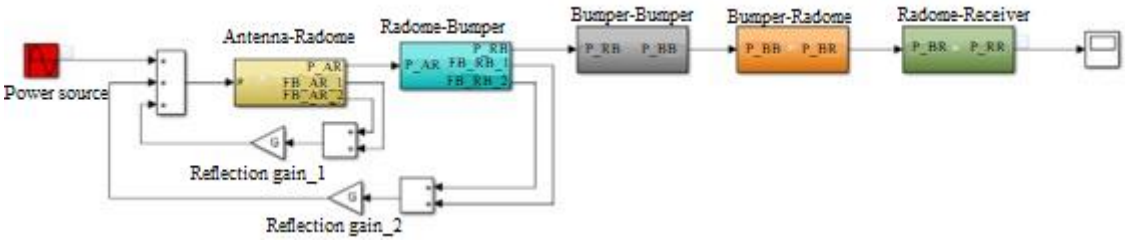

Figure 6.6: Simulink model to evaluate the power losses

The aim of this model is first to understand how much power the radar receives back when their waveforms leave it, pass through the radome and the bumper, reach the target and come back passing again trough the different layers, and the second aim is to evaluate how a proper spacing and dimensioning of the layers influences the power losses. As already mentioned in order to get back reflections in phase with the emitted signal, so that they lead to a constructive interference, the space between two layers and the thickness of each of them has to be a multiple of half of the wavelength. In the first simulation all the layers are considered made of PP, since it resulted the best material

for radar transmission but also because absorption doesn't matter and so evaluate different thickness influence only the back reflection phenomenon. Before showing the results of the simulation is better to understand how the model is built. It is composed of five different subsystems shown in Figures 6.7-6.11.

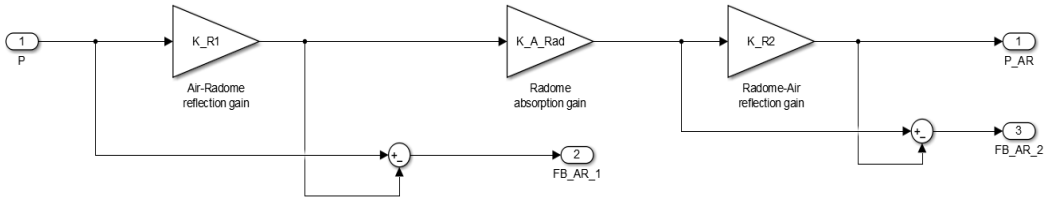

Figure 6.7: Antenna-Radome subsystem

The first subsystem is the Antenna-Radome one and takes into account the reflection when the signal leave air and reach the radome (in the K_R1 gain), the absorption of the radome (K_A_Rad gain) and the reflection when the waveforms leave the radome and go towards air (K_R2). The two feedback FB_AR_1 and FB_AR_2 are respectively the amount of power reflected back towards the radar when the signal enter and leave the radome. These two signals will be multiplied with the reflection_gain_1 G that has a value between -1 and 1. Since it is interesting consider the limit cases the value -1 will be given to G when a wrong design is done which leads to destructive interference between the back reflection and the emitted signal from the radar and value 1 when the design is done in a proper way obtaining constructive interference. In the real installation the amount of power that hit the radar and is reflected again towards the outside has to be estimated in order to attribute to G a proper value. The mentioned gains are obtained considering the reflection and absorption formulas used before to characterize the materials, but considering in this case the single pass transmission and not the double one (and so T and P and not $T^2$and P^2). Table 6.9 shows the value used during the simulations for the gains.

K_R1 (for PP)	K_A_Rad (3.9 mm layer of PP)	K_A_Rad (2.6 mm layer of PP)	K_R2 (for PP)
0.962	0.999	0.999	0.922

Table 6.9: Antenna-Radome subsystem gains

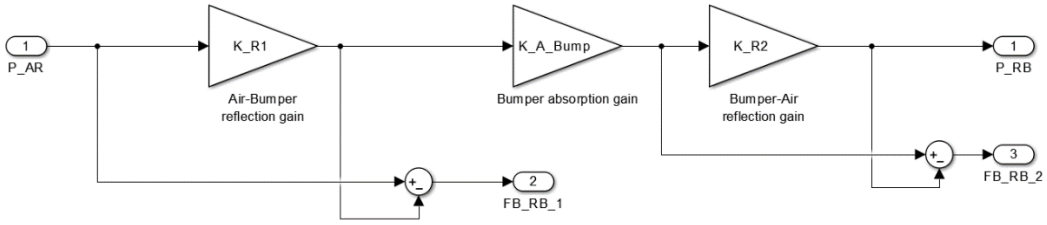

Figure 6.8: Radome-Bumper subsystem

The second subsystem is the Radome-Bumper one and has the same structure of the first one. It takes into account the reflection when the signal leave air and reach the bumper (in the K_R1 gain), the absorption of the bumper (K_A_Bump gain) and the reflection when the waveforms leave the bumper and go towards air (K_R2). Even in this case we have the two feedbacks accounting for reflections, which signals will be multiplied for the reflection_gain_2 G. The same considerations of the previous case hold on. Table 6.10 shows the values used during the simulations for the gains.

K_R1 (for PP)	K_A_Bump (11.7 mm layer of PP)	K_A_Bump (10.4 mm layer of PP)	K_R2 (for PP)
0.962	0.997	0.997	0.922

Table 6.10: Radome-Bumper subsystem gains

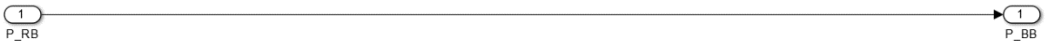

Figure 6.9: Bumper-Bumper subsystem

The third subsystem is the Bumper-Bumper one, shown in Figure 6.9, and takes into account the power losses during the transmission of the signal from when it leaves the bumper of the ego vehicle to when hits the bumper of the target vehicle. It could be modeled considering the main equation of the radar transmission (equation 4.4) and so having an output signal which decreases with increasing distance, but since the thesis is interested only on attenuation and power losses caused by the installation of the radar, this subsystem is left ideal and corresponds to a unitary gain. Another topic could be model it from experimental data in order to simulate the environment attenuation, but it moves away the mentioned aim of the work.

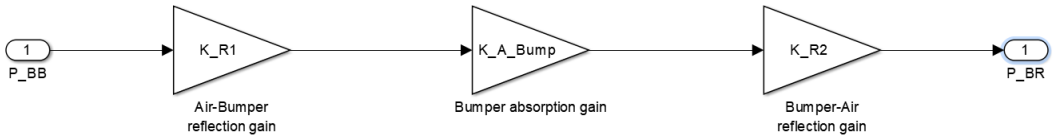

Figure 6.10: Bumper-Radome subsystem

The Bumper-Radome subsystem (in Figure 6.10) is the same of the Radome-Bumper one but without feedbacks. The reason is that even if also in this case when the signal pass from a medium to another reflections occur, they will not come back to the radar but to the target since they are moving from the obstacle to the receiving antennas, and so in any case these reflections will not interfere with the emitted signal. The values of the gains are the same of the ones listed in Table 6.10.

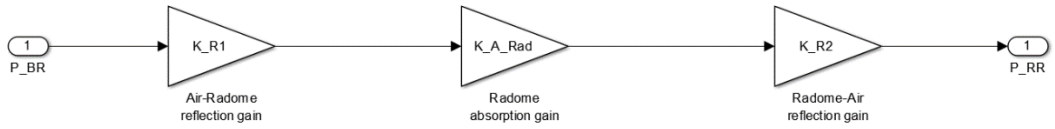

Figure 6.11: Radome-Receiver subsystem

The Radome-Receiver subsystem is the same of Antenna-Radome one but without feedbacks for the same reason explained in the previous subsystem. The values of the gains are the same of the ones listed in Table 6.9.

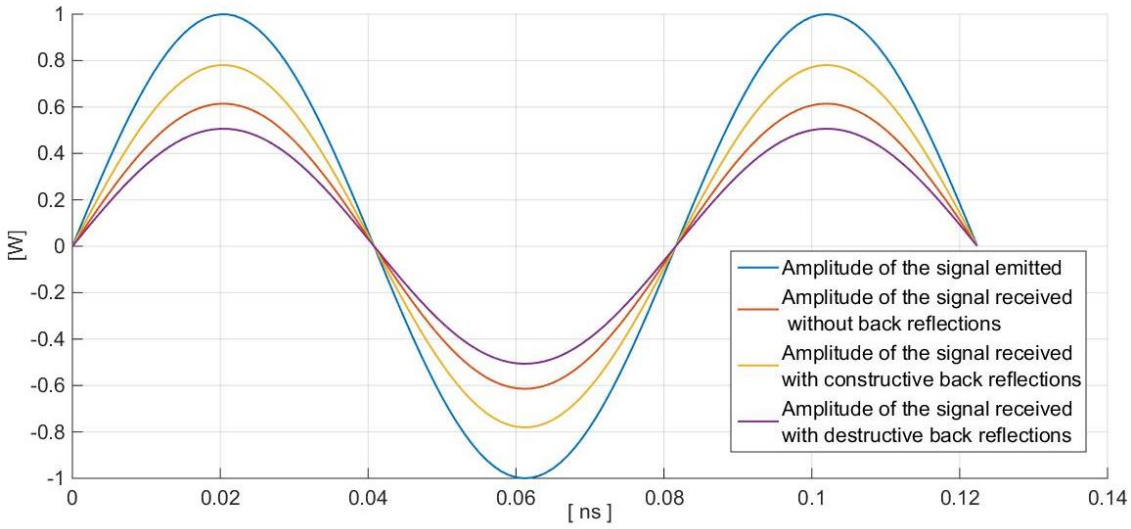

Figure 6.12: Comparison of the received power with the emitted one

Figure 6.12 shows the results in terms of amplitude of the signal received (so the one exiting the Radome-receiver subsystem) in different configurations. The red line represents the received power without considering reflection interferences with the emitted signals, and so is the case in which the reflection gain G is put equal to zero. It is necessary to say that in reality, back reflections always occur and depending on the design of the layers they will be phase shifted with respect to the emitted signal. The yellow line represents the received power in the case of an optimal design, so when the spacing between layers and their width is a multiple of half the wavelength. In the case of PP layers at a frequency of 77 GHz, λ is equal to 2.6 mm. In this case the radome is designed with a width of 3.9 mm (= $3\lambda/2$), and the bumper is 11.7 mm (= $9\lambda/2$). The purple line represents the received power in the worse design, considering spacing between layers and their width as an odd multiple of quarter the wavelength. In this case the radome is designed with a width of 3.25 mm (= $5\lambda/4$), and the bumper is 9.75 mm (= $15\lambda/4$).

It has to be noted that absorption in PP is negligible and so also the power loss caused by it do not changes changing the width of the layers (K_A_Rad and K_A_Bump are the same both in the first and in the second design strategy) and so the difference in the received power is only caused by the back reflections interference phenomenon. Table 6.11 shows the result of the amplitude of the received power with respect to the emitted one in percentage and in dB.

	In %	In dB
Received power neglecting back reflections	69.47	-1.58
Received power with constructive reflections	78.26	-1.06
Received power with destructive reflections	50.75	-2.95

Table 6.11: Received power compared to the emitted one in different configurations

Figure 6.13 shows the results of the second simulation (listed in Table 6.12) that evaluate the power loss in a single pass transmission through radome (of 3.9 mm width made in PP) and bumper (of 11.7 mm width made in PP) properly designed and so consider the power loss in the total path from when the signal leaves the transmitter and reach the air around the bumper.

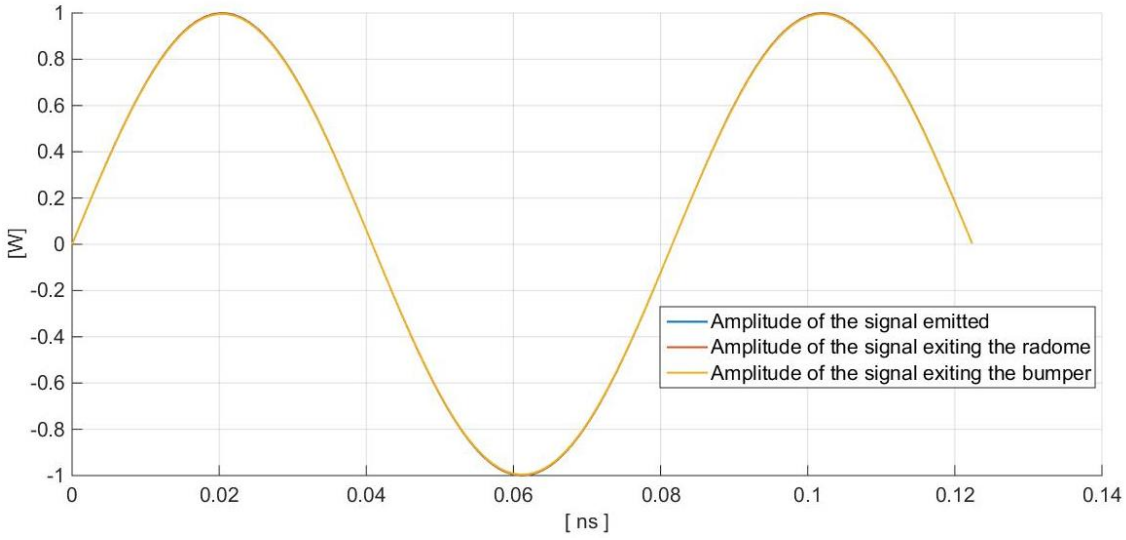

Figure 6.13: Comparison of the emitted power with the ones exiting radome (in PP) and bumper (in PP)

	In %	In dB
Power exiting the radome	99.94	-0.0026
Power exiting the bumper	99.64	-0.0157

Table 6.12: Power exiting radome (PP) and bumper (PP) compared to the emitted one

The results listed in Table 6.11 demonstrate the benefit of having a proper dimensioning and spacing of radome and bumper, receiving a signal with the 78.26% of the emitted one, while in the worse design the percentage is equal to 50.75%. It has to be said that these are limit cases, since in a real implementation only part of the reflected back signal will be again reflected in the correct direction and so the reflection gain will not be G=+-1 as it would be if the radar chip surface were a mirror. In a real case 0<|G|<1 and so the two percentages will be closer.

The results of Table 6.12 instead show that if the layers are done in PP and so absorption can be neglected, designing properly radome and bumper, the power of the signal exiting the ego vehicle would be almost the same of the emitted one by the radar. Comparing Figure 6.13 with Figure 6.12 (the yellow lines), it can be noticed that all the power losses occur in the coming back path from when the waveforms hit the obstacle to when they reach the receiver, since almost no losses appear in the path from the transmitter to the air around the bumper. Also, in this case this is not completely true if 0|G|<1 as it would be in a real case. This last phenomenon is not even true if we consider radome and bumper made of PC in which absorption is no more negligible.

Table 6.13 shows the gains used in the Simulink model for this third simulation.

K_R1 (for PC)	K_R2 (for PC)	K_A_Rad (3.6 mm layer of PC)	K_A_Bump (10.8 mm layer of PC)
0.945	0.910	0.911	0.755

Table 6.13: Simulink model gains

It has to be underlined that for PC λ=2.4 mm and so the dimensions of the layers in order to have a proper design are set equal to 3.6 mm (= 3 λ/2) for radome and 10.8 mm (= 9 λ/2) for bumper.

The results are shown in Figure 6.14 and listed in Table 6.14.

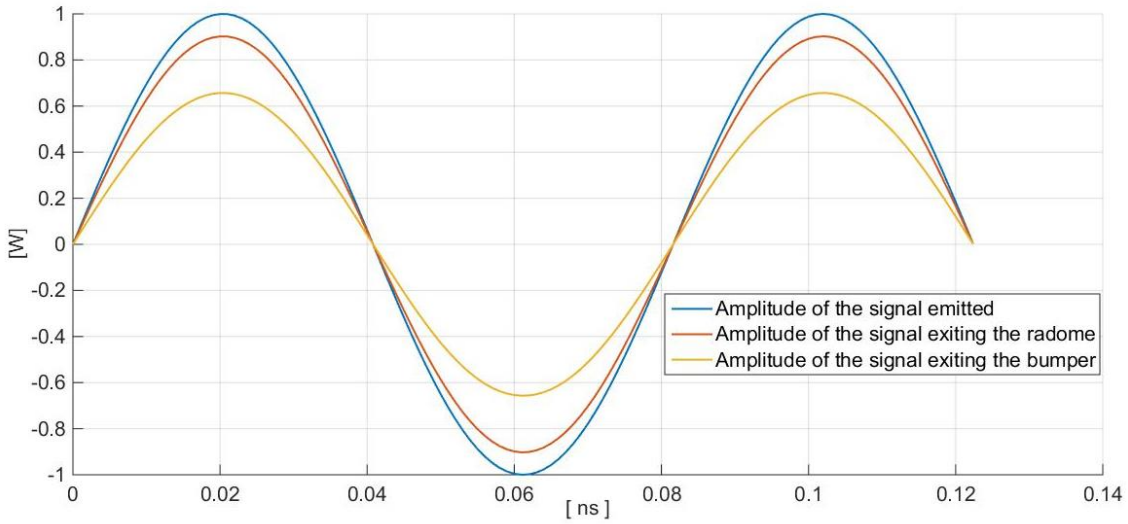

Figure 6.14: Comparison of the emitted power with the ones exiting radome (in PC) and bumper (in PC)

	In %	In dB
Power exiting the radome	90.27	-0.445
Power exiting the bumper	65.70	-1.824

Table 6.14: Power exiting radome (PC) and bumper (PC) compared to the emitted one

Using PC, as shown in Table 6.14, power losses occur also in the path from radar to the air outside bumper and this is due to the higher absorption of PC respect PP.
Simulations done in this chapter underline that PP is the best material to build radomes and bumpers and a proper choose of the spacing and dimensioning of them lead to a better transmission. PC is also good for radome since a thickness around 3 mm do not lead to higher absorption, but if it has to be used also for bumpers their thickness have to be as low as possible. In order to have not this constrain for bumper design PP is suggested.

Chapter 7

7. Angle error introduced by curved radomes and bumpers

In the previous chapters different aspects regarding the choice of the radome and bumper materials, the dimensioning of these layers and the spacing between them were analyzed. In this chapter considerations about the shape of the surfaces in front of the radar are considered in order to evaluate the angle error introduced to the incident rays depending on the curvature of the surface itself [24], [25].

As proved by the Snell's law and shown in Figure 5.5, when a radar beam hit a surface the direction in which it will be transmitted will not be in general the same of the incident beam. This introduction of an angle error occurs whenever a signal is transmitted in a different medium hitting the surface not perpendicularly. As first result we obtain that to moderate this phenomenon is better to design the layers in such a way they will be as perpendicular as possible to the incident beams. In the presence of a flat surface, Snell's law is sufficient to evaluate the angle error introduced, while for curved ones it has to be derived considering more parameters as the distance from the source to

the surface and its curvature.
This is what will be done here evaluating the phenomenon both for concave surfaces (and so simulating how rays exiting curved radomes or bumpers are deflected) and convex surfaces (observing how rays deflection occurs when signals come back toward the radar). It has to be said that in order to avoid these complications during the design process, it is better to put radar behind flat surfaces, but sometimes radomes are curved and also the bumper area above the radar can have a certain curvature and this motivate the choice of analyzing this aspect.

7.1. Angle error in concave surfaces

Let consider a concave surface as shown in the Figure 7.1.

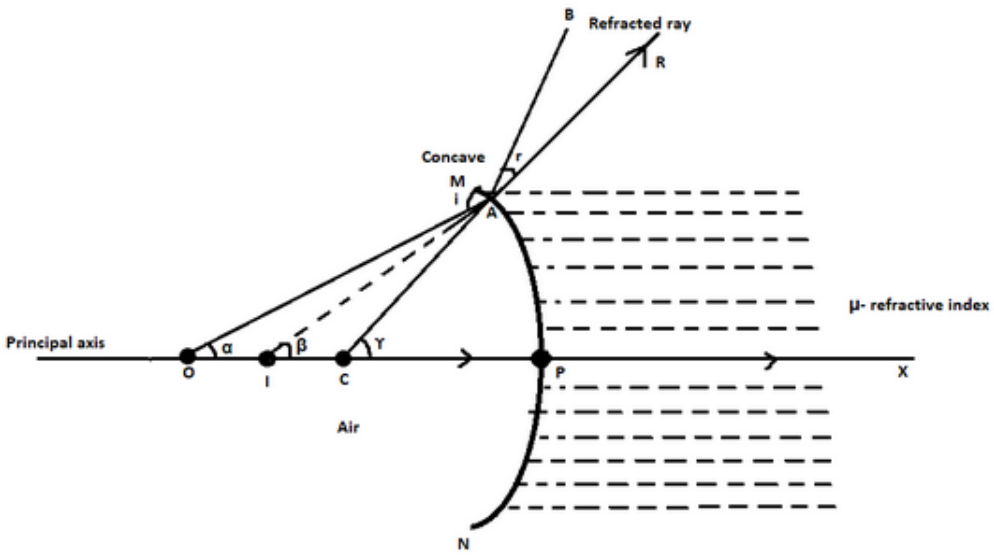

Figure 7.1: Diagram for evaluate angle error in a concave surface, from [24]

The surface is represented by MPN . The refractive index of the medium of the surface is μ. Consider P as the pole of the surface, O as the center of curvature, while PC is the principal axis of the refractive spherical surface. Consider a point object at O (where the radar is). An incident ray travels through C and it is perpendicular to the surface. It will

not undergo any refraction and so it will travel in a straight line along PX . Another ray that need to be considered is OA . It will refract at the point A bending towards the normal. At a point i we will have a virtual image.
Consider the ray angles with the principal axis to be α, β and γ respectively.
By using exterior angle theorem in ΔIAC , we get:

$$\gamma = \beta + r \qquad (7.1)$$

And from this:

$$r = \gamma - \beta \qquad (7.2)$$

Where r is the angle error introduced by the concave surface. For a spherical surface, we can write the angle as:

$$\text{angle} = \frac{\text{arc}}{\text{radius}} \qquad (7.3)$$

And so:

$$\beta = \frac{PA}{IP} \qquad (7.4) \qquad \gamma = \frac{PA}{CP} \qquad (7.5)$$

Now let apply the sign convention:

PC = − R (where R is the radius of curvature)
PI = − v (where v is the distance of the image from the pole of the surface)
PO = − u (where u is the distance of the object from the pole of the surface)
PA = $-u * \sin(\alpha)$ (where u is the distance of the object from the pole of the surface and α is the incidence angle)

And so, deriving v from the main expression of the refraction at concave spherical surface that is:

$$\frac{\mu-1}{R} = \frac{\mu}{v} - \frac{1}{u} \qquad (7.6)$$

r can be evaluated as:

$$r = -\frac{u*\sin(\alpha)}{R} + \frac{u*\sin(\alpha)}{v} \qquad (7.7)$$

The results are shown in Figures 7.2-7.4, considering different radii of curvature and distances and an angle of incidence that spans from -45° to 45°.

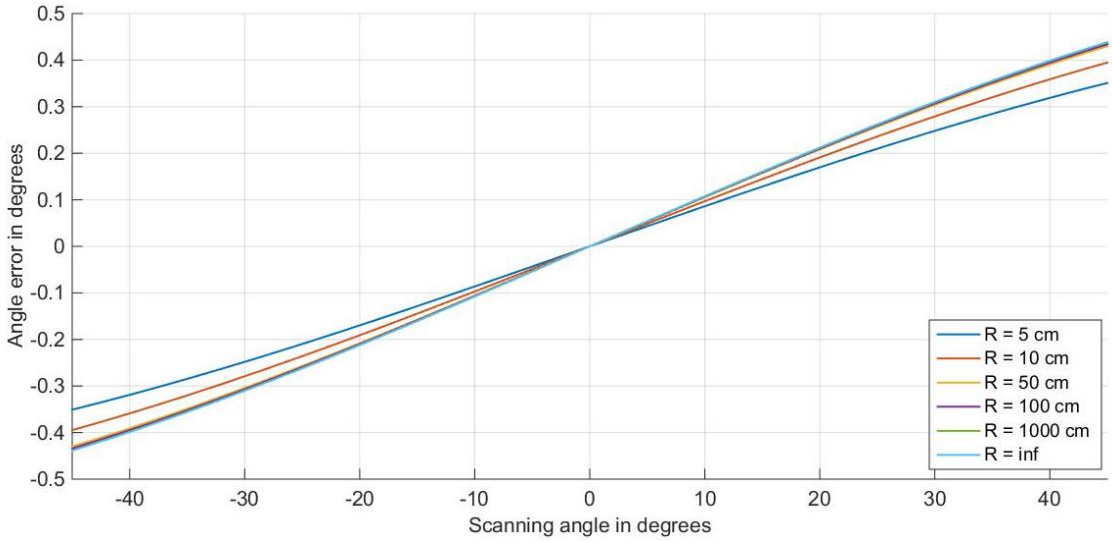

Figure 7.2: Angle error for different concave curved surfaces at 1 cm from radar

The result shows that increasing the radius of curvature R the angle error increases as well, till approaching to a limit curve that indicates the angle error when the incidence rays hit a flat surface (R=inf). For concave surfaces the error is positive when the incidence rays are inclined with a positive angle and is negative when the incidence angle is negative. For +-45°, that represent the extremes of the considered field of view, the maximum error is in absolute value equal to 0.4385°. It seems not a big value but a long-range distance radar is able to sense an obstacle hundreds meters far away and so even this small angle is enough to see for example a car that is in the same lane of the

ego vehicle as it was in the adjacent lane. It has to be noted that these curves are obtained considering PC as the material of the surfaces. They are material dependent since, in the equations used to obtain them, appear the refractive index that changes changing material. If PP is considered, at +- 45° the maximum angle error for a flat surface would be in absolute value 0.4767°.

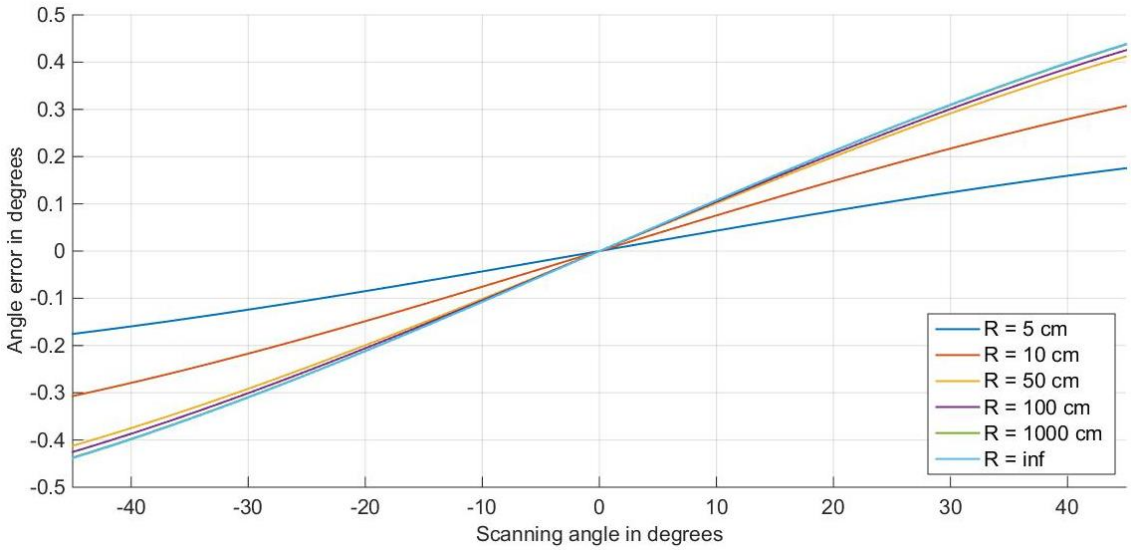

Figure 7.3: Angle error for different concave curved surfaces at 3 cm from radar

Comparing Figure 7.3 with Figure 7.2, it can be seen that increasing the distance from the center of curvature of the surface, to tend to the limit curve an higher radius is needed. In the previous case in fact with a radius of 50 cm the curve obtained (the yellow one) almost overlap the limit one (in cyan) while in this second case even with the curve of 100 cm (the purple one) it is possible to see it separate from the limit one, and this demonstrate that what is important is the ratio between the radius and the distance.

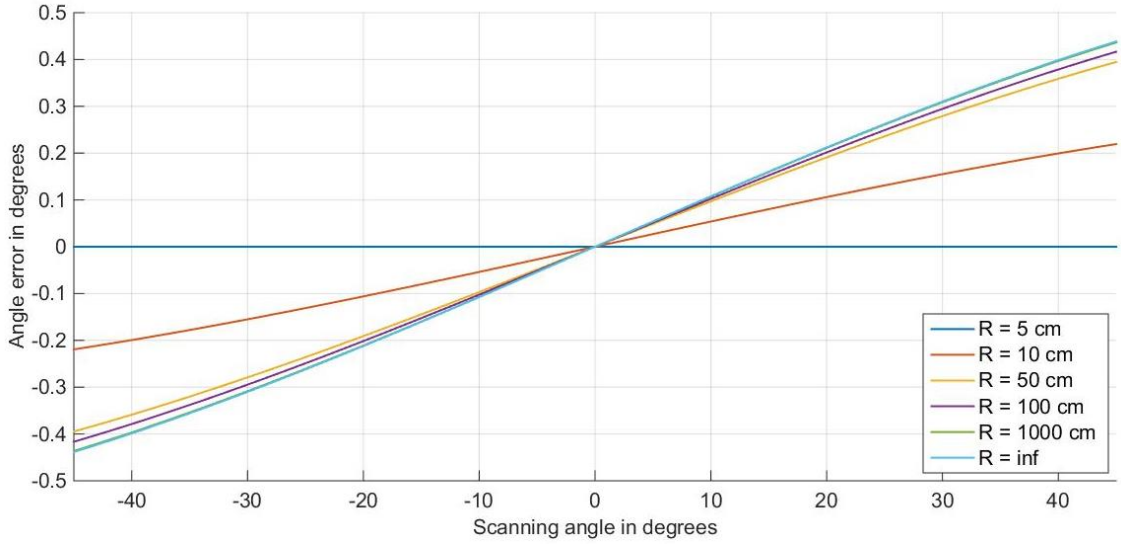

Figure 7.4: Angle error for different concave curved surfaces at 5 cm from radar

Figure 7.4 shows the same trend of the previous ones and the same considerations hold on but is interesting to note that considering a distance of 5 cm from the center of the curvature with a radius as well of 5 cm, the angle error is always 0° independently from the incidence angle. In this case in fact the source coincides with the center of the curvature and all its rays will be always perpendicular to the surface and if it happens, as demonstrated with the Snell's law, the angle error is 0°.

7.2. Angle error in convex surfaces

For convex surfaces the same reasonings done for the concave ones hold on, but in this case the sign convention changes. In order to understand it, Figure 7.5 is shown.

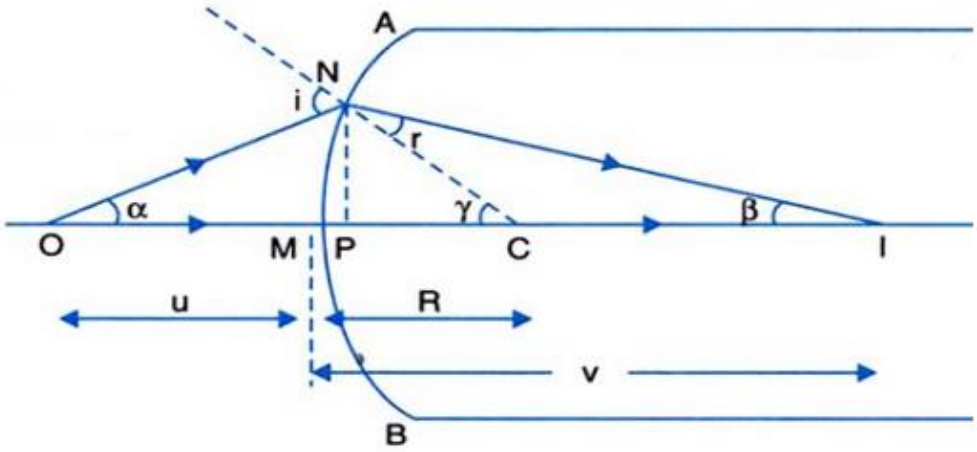

Figure 7.5: Diagram for evaluate angle error in a convex surface, from [25]

In this case in fact the sign convention is:

PC = R

PI = v

PO = − u

PA = − u ∗ sin(α)

And so, r can be evaluated as:

$$r = \frac{u*\sin(\alpha)}{R} - \frac{u*\sin(\alpha)}{v} \qquad (7.8)$$

The results are shown in Figures 7.6-7.9, even in this case considering different radii and distances and an incidence angle that spans from -45° to 45°.

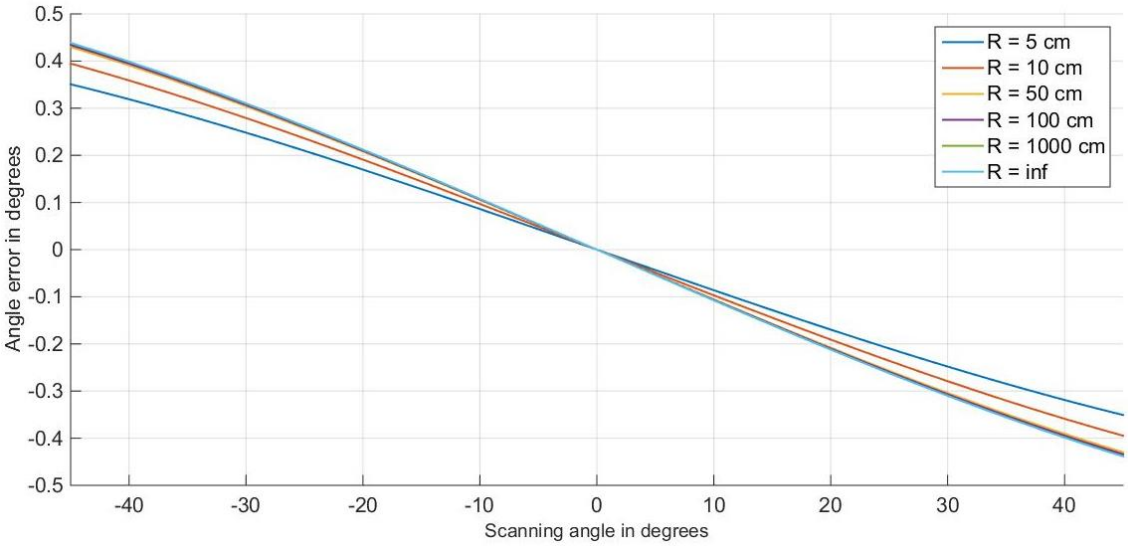

Figure 7.6: Angle error for different convex curved surfaces at 1 cm from radar

The results are symmetrical to the concave case, the limit values are the same in absolute value but in this case the angle error is positive when the incidence angle is negative and vice versa.

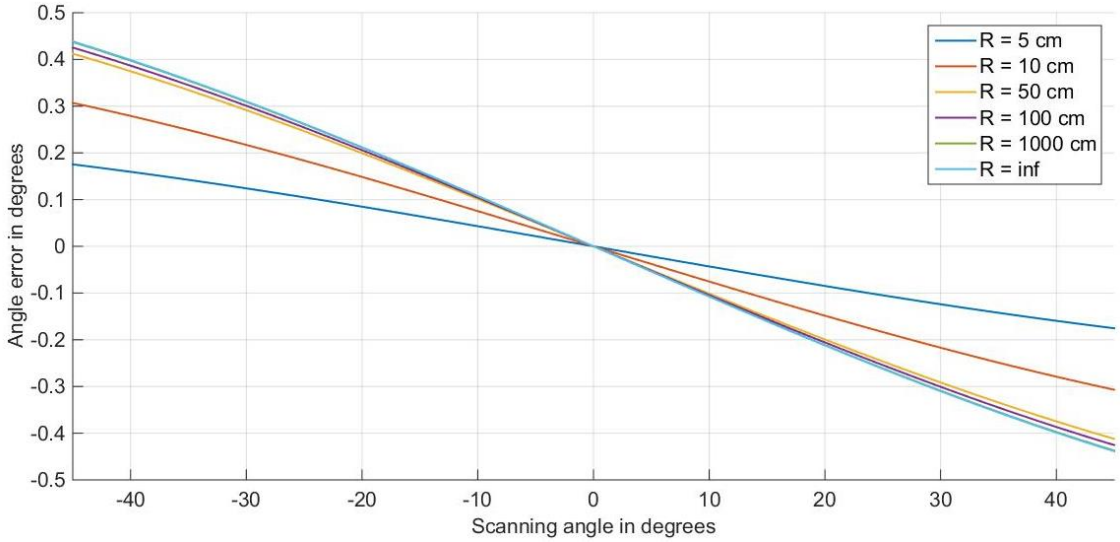

Figure 7.7: Angle error for different convex curved surfaces at 3 cm from radar

Figure 7.7 shows that even in the convex case the angle error curve will tend to the limit one as much faster as the ratio between radius of curvature and distance is higher.

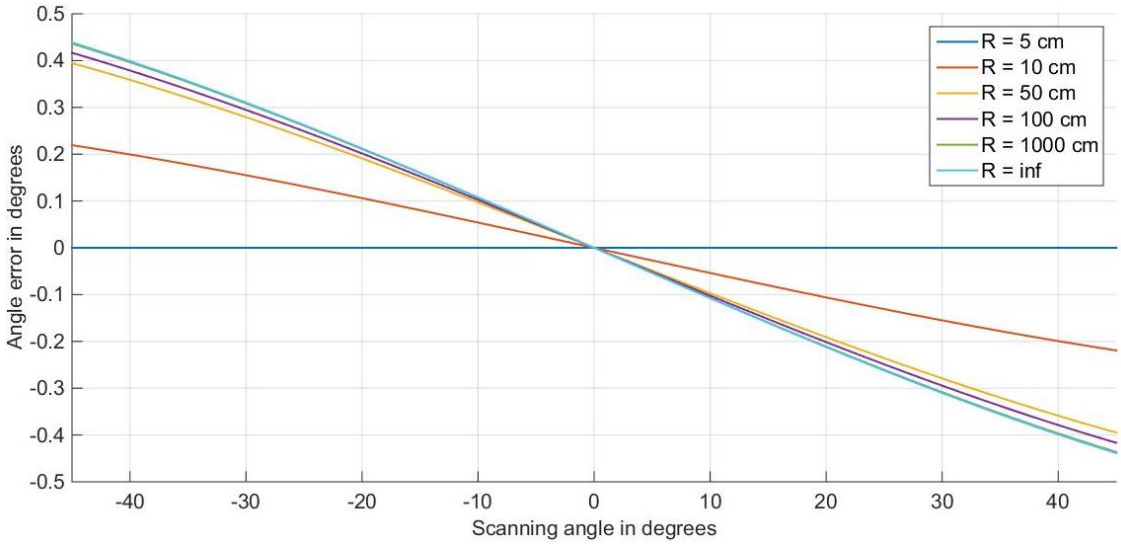

Figure 7.8: Angle error for different convex curved surfaces at 5 cm from radar

As it can be seen in Figure 7.8 when analyzing the curve obtained taking into account a surface with curvature of 5 cm set at a distance of 5 cm to the source, even in the convex case if the distance and the radius are the same no angle error occurs independently on the incidence angle.

It has to be underlined that these curves are obtained considering the center of curvature to belong to the same axis that pass also from the source point. If is not the case, evaluate the angle error is even more complex and electromagnetic simulation are strongly suggested. Having the source in the same axis of the center of curvature is not a mild constraint and in the opposite case angle errors can reach higher values then the presented ones. This is the reason why flat surfaces are preferable. In this case in fact the evaluated limit curves hold on even in the case in which the source is shifted with respect to the center of curvature (think about a circumference with infinite radius, changing the position of the center, the circumference will always have an infinite distance to the center in all its point).

Since the FOV used in long range distance radars do not cover +- 45° but is narrower, Table 7.1 shows the limit angle error in absolute value both for PC and PP surfaces for +-3°, +-5°, +-10° FOV.

	For PC surface	For PP surface
Maximum angle error FOV 3°	0.0325°	0.0353°
Maximum angle error FOV 5°	0.0541°	0.0587°
Maximum angle error FOV 10°	0.1077°	0.1171°

Table 7.1: Maximum angle error for flat surfaces changing FOV

It can be appreciated from the results listed in Table 7.1, and also observing the graphs, that for low angles the maximum angle error increases almost linearly increasing the incidence angle, this approximation can be used to evaluate the maximum angle error for all the long-range distance radar FOV that are always less of +-10°.

Chapter 8

8. Simulation on the positioning of radar sensor through AV Simulator

In the previous chapters considerations about the installation of the sensor in the front of the car were done. Is also interesting evaluate how the position of the sensor can influence its performances and this is what is done in this chapter. To do that simulations using an automotive simulator (ScanerStudio) are performed. In the next paragraph is presented a description of the software used while in the following ones two different analysis are carried on. The first considers a normal operation on the radar that has to perceive a car in its same lane, evaluating if different positions lead to a different perception. In this section will be evaluated also the limits of the used software. In the second simulation a cut-in scenario is provided evaluating the benefit of an horizontal shifting of the radar position.

8.1. Description of the software used

SCANeRStudio is a driving simulation software. It is used for advanced engineering studies as well as for road traffic research and development. It is also helpful for human factor studies and driver training.
SCANeRStudio offers 5 main modalities:
• Vehicle mode: For generating any mathematical model of a vehicle. Models are based on components (such as: shock, brakes, lights, tires, wheels).
• Terrain mode: For generating a road network including logical information (such as: signs, traffic lights, speed limits) and including a 3D graphical environment.
• Scenario mode: For generating exercises based on vehicles and terrain in order to improve: a driver, a road infrastructure or cockpit commands. This mode is also for: tailoring situations, managing autonomous vehicles around the driver, asking to respect instructions and getting some mathematical measurements.
• Simulation mode: For launching an exercise and handling all the simulator modules. The simulator is composed of hardware and software for sound, visualization and motion. SCANeR modules are processes that handle such hardware and software.
• Analysis mode: For analyzing the results of the exercises (graphs, 3D animations, datasheets).

The simulations presented in the following paragraphs are implemented considering vehicles and terrains already present in the available libraries, while the scenarios are customized in base of the aim of the simulations that are performed taking advantages of the simulation mode of ScanerStudio as well as the results are investigated through the analysis mode and the interface of the software with Matlab & Simulink.

8.2. Positioning of the radar in an ordinary scenario

In the first simulation an ordinary scenario, shown in Figure 8.1, is presented in which the ego vehicle is equipped with a radar installed in the front bumper (without

considering the attenuation of the installation in order to evaluate only the position related aspects), in different configurations, changing the position both in the vertical axis (considering three different altitudes) and in the horizontal one (putting the radar in the extreme right of the bumper, in the middle and in the extreme left). The scenario provides a target vehicle in the same lane of the ego vehicle that is stopped and at the beginning outside the field of view of the radar.

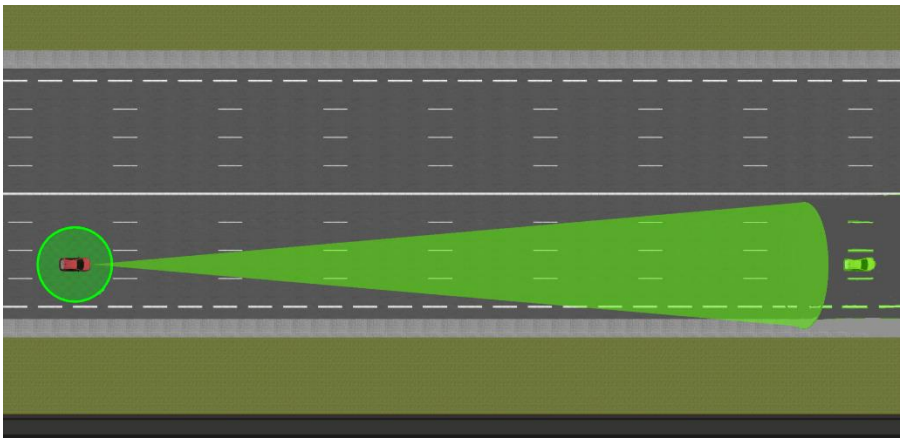

Figure 8.1: Scenario representation

The ego vehicle instead is driven autonomously by the software and it starts braking when detects the obstacle as too close, till stop itself completely. The simulation's aim is to understand if the variable of interest, as relative distance and relative velocity to the target, are influenced by the position of the radar. Figure 8.2 shows the velocity that the ego vehicle maintains during the simulation.

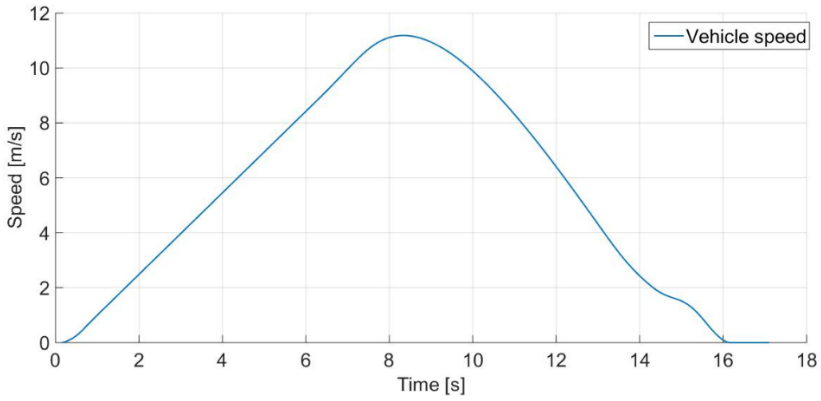

Figure 8.2: Ego vehicle speed

The sensor parameters are an horizontal FOV that spaces from a minimum angle of -5° to a maximum angle of +5° and a vertical FOV that spaces from a minimum angle of -10° to a maximum angle of +10°. The maximum range in which it can detect an obstacle is 85 m**.**

First the changing of the horizontal position is performed. The front side of the ego vehicle has a length of 1.8 m and the sensor is set in the extreme left (-90 cm), in the middle (0 cm) and in the extreme right (+ 90 cm), leaving the altitude of the sensor fixed to 50 cm from the ground. The results in terms of sensed relative distance and relative velocity are shown in Figures 8.3, 8.4 respectively.

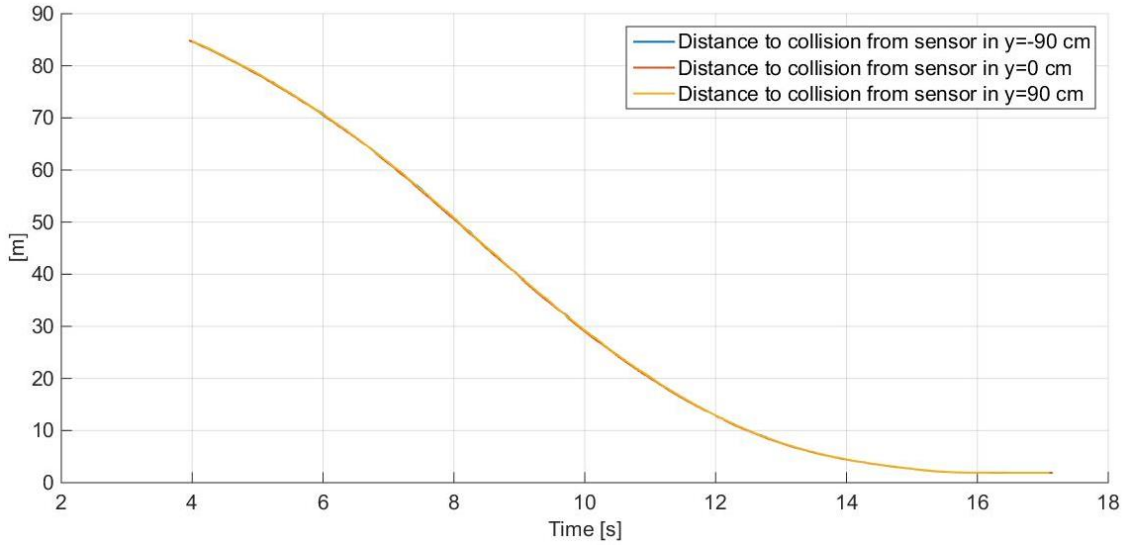

Figure 8.3: Distance to collision perceived by the sensor set in different horizontal positions

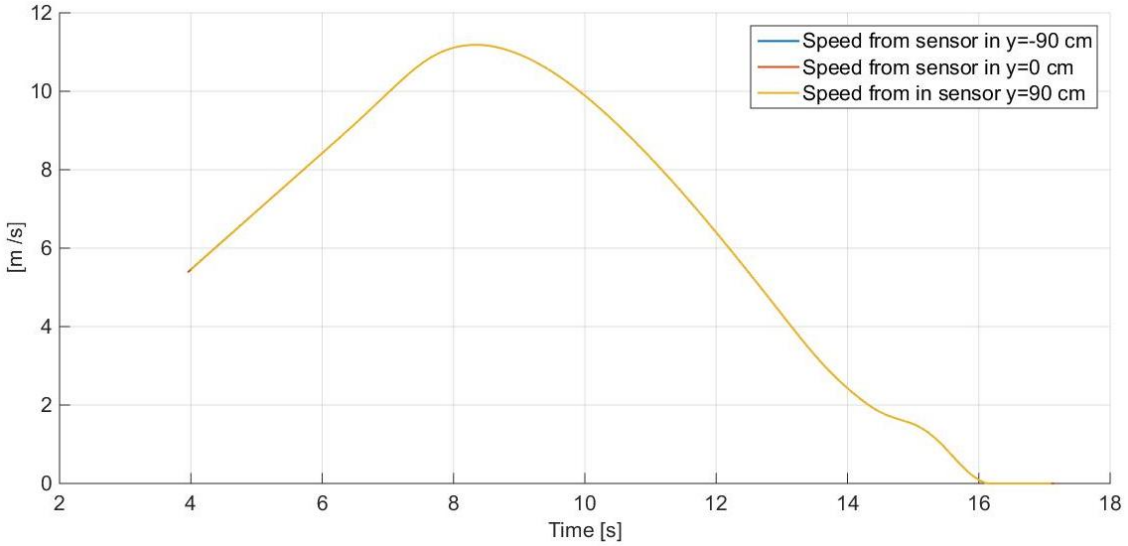

Figure 8.4: Relative speed perceived by the sensor set in different horizontal positions

The results show that the different curves obtained changing the position of the radar through the horizontal axis, almost overlap having an error of few centimeters between them that is reasonable due to the fact that changing the position of the radar the nearest point of the obstacle will have a distance slightly different. It can be seen comparing Figure 8.4 with Figure 8.2, that from when the target enters in the FOV of the radar the velocity (and the distance) perceived coincides with the true one having no significant shifting changing the position. The error that derives from these settings is as much smaller as the target is much more distant from the ego vehicle, but even when it approaches the obstacle and stops (with a true relative distance of 5 m) it is negligible.

Same analysis is performed changing instead the vertical position. The sensor is set with an altitude of 20 cm, 50 cm and 100 cm from the ground, leaving the horizontal position of the sensor fixed in the middle position (0 cm). The results in terms of sensed relative distance and relative velocity are shown in Figures 8.5, 8.6 respectively.

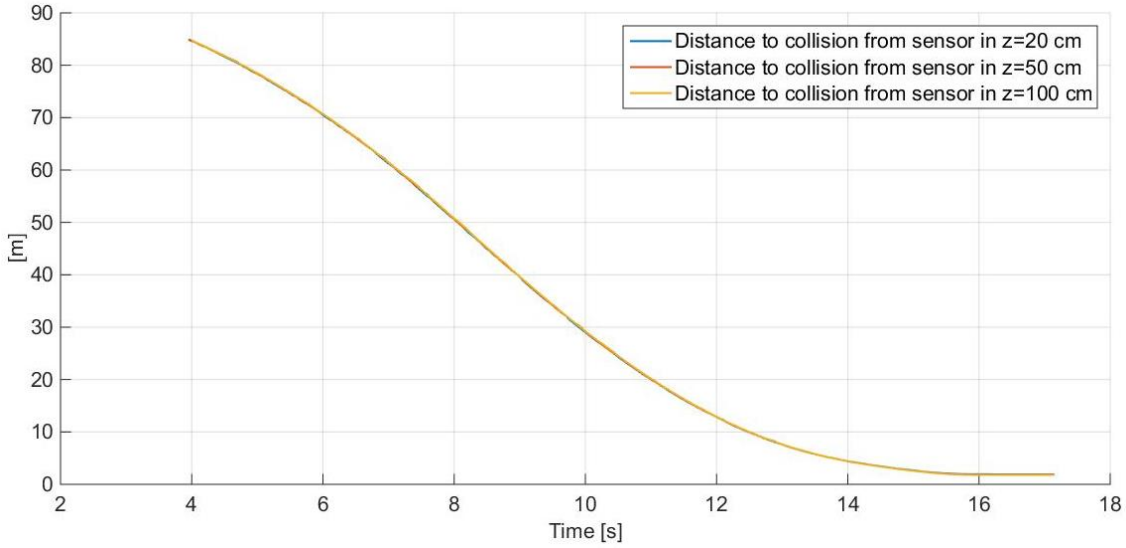

Figure 8.5: Distance to collision perceived by the sensor set in different vertical positions

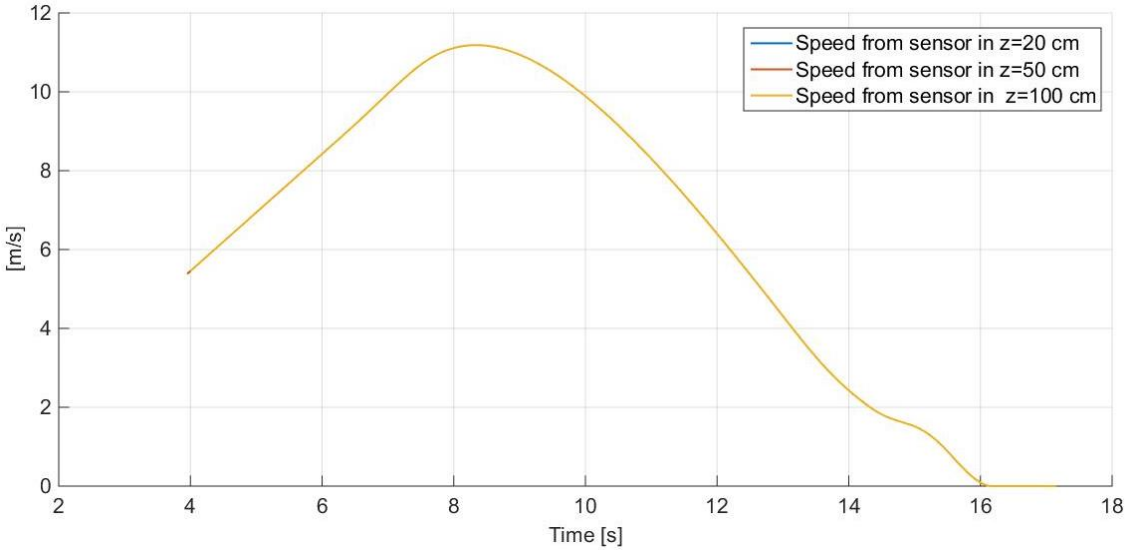

Figure 8.6: Relative speed perceived by the sensor set in different vertical positions

The same considerations expressed for the horizontal shifting hold on even for the vertical one, having no considerable changing moving the sensor. It has to be said that if the results shown in Figures 8.3, 8.4 were expected since it is only a matter of when the obstacle enters in the FOV and how far the nearest point of it is detected, it seems that the results obtained changing the altitude have a certain degree of ideality. In fact, in this case an always present constraint is the road and changing the altitude of the sensor

would be possible having different results since if the radar is located too close to the ground, noise coming from the signal's reflection when ground is hit could be higher. However, ScanerStudio is a system-level-simulator software and not a physic-based-simulator software and it doesn't consider phenomena like reflection of the signal on the road and its consequently power loss. Investigation about this phenomenon is needed even if, observing the solution provided by the principal carmakers in which very usually the sensor is set in the lower part of the bumper, it does not seem a big constraint. In fact, in the case in which the signal is noisier, the signal-to-noise ratio SNR that appear in the main equation (4.4) of radar systems will be lower and so the power of the received signal that hit an obstacle at a distance d and comes back will be lower as well. Since the power threshold under which the radar is not more able to work properly is fixed, it means that it can do its job till a distance $d1<d$.
But considering post processing techniques, this lowering of the maximum distance at which radar can sense, is not so huge and this is the reason why even lower position are often considered.
However, before getting the conclusion that this aspect cannot be evaluated through the used software, a simulation introducing noise was done but the noise that is introduced by ScanerStudio on the signals is a random white-noise and it is only noise added to the output signal instead of evaluate the output signal in a noisy environment.
In order to prove that the noise introduced is completely random and do not depend on the different position, for each configuration a second noisy distance to collision is evaluated maintaining exactly the same scenario and even in this case evaluating the infinity norm of the difference between the sensed distance and the real one, these norms result different. This last simulation does not provide any advantage into evaluating radar positioning but is anyway presented to underline this limit of the used software.
Considering the conclusion the ScanerStudio do not takes into account physical aspects as reflection and power losses of the signal, it would be not useful evaluate the positioning of the radar in even more complex and rich scenarios then the presented one, but since instead geometrical aspects and considerations about how the configurations of the sensor influence the time instant in which an obstacle enters in the field of view and consequently how much time it can be gained to take actions, another

simulation is done and presented in the next paragraph in which investigation on the horizontal shifting of the radar and its advantages in the cut-in maneuver are presented.

8.3. Positioning of the radar in a corner case scenario: the cut-in maneuver

Cut-in maneuvers occur when vehicles change lane and move closely in front of a vehicle in the adjacent lane. They are very common but adversely affect roadway capacity and traffic safety. The choice of simulate this scenario is taken because it is one of those that mostly influences the perception of the surrounding environment changing the horizontal position of the radar. The reason is that since the vehicle comes from behind the ego vehicle, it will approach and enter in the FOV near to the starting point of it and so when it covers not a huge area. Imaging the covered area as a cone, the cutting in vehicle enters in a dangerous area very near to the vertex of the cone (that corresponds to the position in which is set the sensor) and so shifting it, could lead to different perceptions. In order to better understand it Figure 8.7 shows the cut-in maneuver.

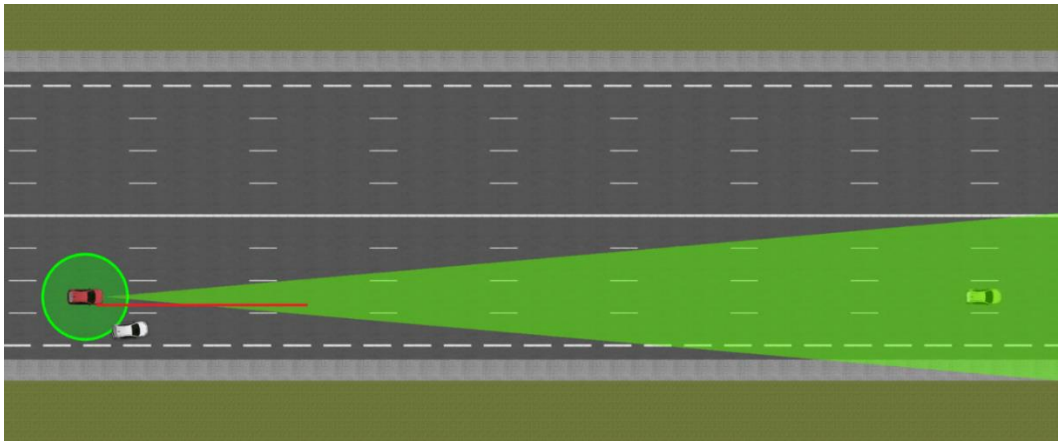

Figure 8.7: Cut-in scenario

In the illustrated scenario there are two vehicles in the same lane at a distance of 93 m

and moving at the same speed (that varies depending on the considered simulation). The second one (the green car) is already inside the FOV of the ego vehicle equipped with a long-range detection radar. A third vehicle (the white one) is cutting in the lane of the ego vehicle approaching with the same speed of the other two and with a certain angle of inclination α with respect to the road (that can represent a variable strictly related with the steering angle). The maneuver is designed is such a way that the ego vehicle and the cutting in one never hit themselves but is however a risky one considering that at the starting point the COG of the two vehicles have a longitudinal distance of 5.9 m between them, and so when the car enters in the lane they will be in a dangerous situation. To be precise in the following simulations the maneuver starts to be risky from the time instant in which the white car enters in the red line represented in Figure 8.7 that is tangent to the extreme side of the ego vehicle and represent a border over which the cutting in vehicle will enter in an area in which the trajectory of the ego vehicle falls. Depending on the position of the sensor, the point in which the car touches this line could be inside or outside the FOV. If it is inside, the perception of a dangerous situation is effectively the one described before, but if it is outside, since it is considered that the ego vehicle can perceive the surrounding environment only thanks to the radar, the instant in which it can be noted that a dangerous situation is occurring is the first one in which, once overtaken the red line, the cutting in car is entering the FOV. It can be resumed that the ego vehicle considers a dangerous situation the first time instant in which, once overtaken the red line, the cutting in car enters in the FOV. Considering the dimensions of the cars, the entering vehicle will touch the red line when it travels a lateral distance of 0.9 m (when simulation starts there are 0.9 m of lateral distance between the closest points of the two cars). In order to evaluate the benefit of the shifting of the position on the lateral axis, two variables can be considered. The first one is how much time the ego vehicle has to react when it senses the object in a dangerous situation. The second one is the time headway that it has. The time headway (Th) is defined as the ratio between the distance to collision and the velocity of the ego vehicle. Considering Figure 8.8 the distance to collision will be 93 m till the white car enters in the perceived dangerous situation, then it will be the distance between the ego vehicle and the cutting in one. The time instant in which the entering car will be sensed as dangerous depends on three main parameters: The FOV, the inclination angle α and the

considered velocity. Figure 8.9 shows an example of time headway in the case in which FOV=+-10° , α=3°, speed= 100 km/h and the sensor is put in the middle lateral position (y=0). In this case no braking action is taken when the obstacle is perceived as dangerous.

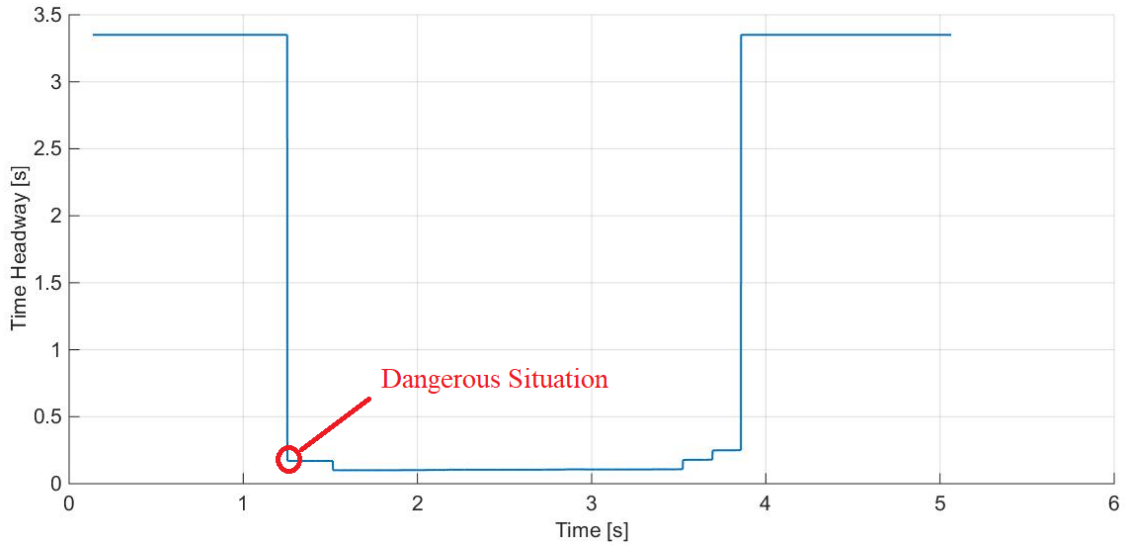

Figure 8.8: Example of the variation of time headway

In the figure above, in the first part the ego vehicle is running at 100 km/h and senses as the nearest target the green vehicle in its same lane that is running with the same speed a 93 m distance, consequently and after converting the speed in m/s , the time headway is of 3.35 s. After 1.25 s from the beginning of the simulation the white car is perceived as dangerous and its distance from the red car is 4.72 m, consequently the time headway for the ego vehicle, that in this example doesn't brake and maintain a 100 km/h speed, falls to 0.17s. In the lower part of the graph the steps that appear are due to the fact that, depending on the maneuver, the nearest point sensed by the radar will change and so its distance. These steps are in any case related to the dimensions of the entering car. In this simulation the cutting in car continues its run with the same inclination angle and so exits the lane and after 3.86 s exits also from the FOV so that the ego vehicle senses again as the nearest target the green car. In this graph the point of major interest is the one circled in red, that as said represents the time instant in which the cutting in car is sensed as dangerous as defined previously. From now on it will referred to this point

calling it the “risky point” and the following simulations search to evaluate the coordinate of the risky point in terms of time headway (the y coordinate) and the time needed to enter in this situation (the x coordinate).
As said before the risky point coordinates depend on the FOV, the inclination angle α and the speed, so first of all considerations about these variables will be derived. In the following simulations three different configurations of the sensor are considered evaluating the data obtained when the radar is set in the extreme right of the bumper (-83 cm), in the middle (0 cm) and in the extreme left (83 cm) considering a car with total lateral length of 168 cm.

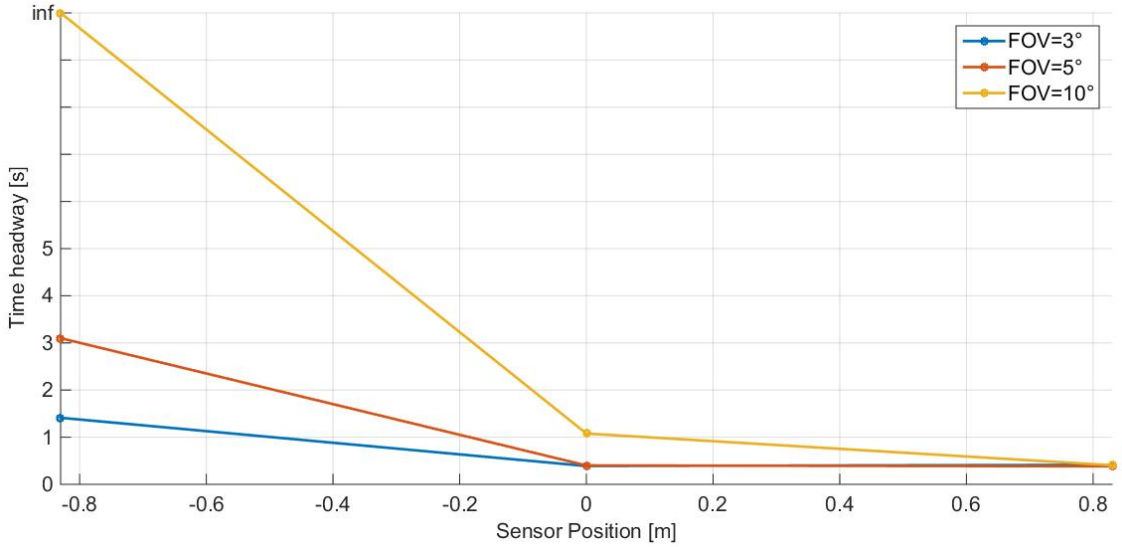

Figure 8.9: Time headway in the risky point considering three different sensor positions varying the FOV

Figure 8.9 shows the dependence of the time headway on the FOV. In this simulation the vehicles are running with a speed of 50 km/h and the entering one has an inclination angle of 3°. The results need to be read considering in parallel Figure 8.10 that shows the time difference expressed as the time in which the cutting in car enters in the FOV minus the time in which it enters in the dangerous situation (the real one not the perceived one, so exactly when the car touches the red line shown in Figure 8.7).

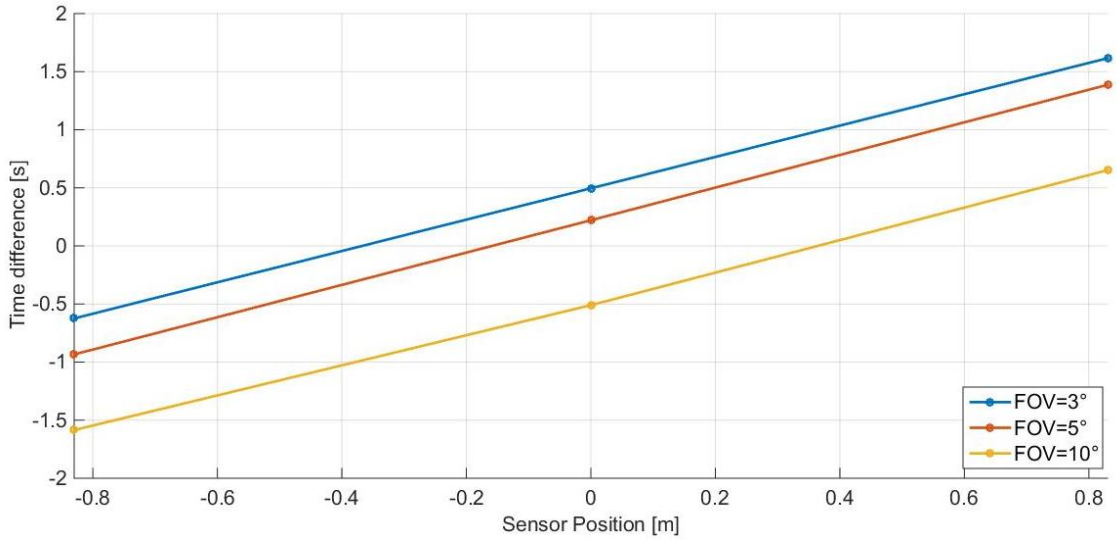

Figure 8.10: Time difference considering three different sensor positions varying the FOV

If the radar has a +-10° FOV and is set in the extreme right position (x = - 0.83 m) and so the closest to the entering car, from Figure 8.10 it can be seen the white car is entering in the FOV 1.59 s before entering in the dangerous situation. In this case the ego vehicle has enough time to brake and stop itself completely, considering an emergency brake deceleration of 9.8 m/s^2, and so when the car enters in the dangerous situation the ego vehicle is already stopped and so as can be seen in Figure 8.9 its time headway evaluated in the risky point is equal to infinite (remembering that time headway has velocity on the denominator). If the sensor is instead set in the center of the bumper (x = 0 m), the time difference will be – 0.51 s (so 0.51 s between entering the FOV and the entering in the dangerous situation), the sensor is even in this case able to perceive the obstacle in advance but not enough to have a complete stop and the time headway in the risky point is 1.08s. Putting the sensor on the extreme left (x = + 0.83 m) bring to a time difference of +0.65s , so that the ego vehicle recognizes a dangerous situation when it happened 0.65 before, so it has no time to take a braking action and the time headway will be 0.40s.

Considering instead a FOV of +- 5° for the three different installation positions, the results really change. In fact for x = - 0.83 m, there is a time difference of -0.93s that differently from the previous case is not enough to completely stop the ego vehicle that will have a time headway in the risky point of 3.1s, for x = 0 m if previously the time

difference was negative, now is positive and equal to 0.22s and so no braking action has time to occur and the time headway is 0.40s as well as it was with FOV=+-10° but in the extreme left position. For x = + 0.83 m the time difference is 1.39s and the time headway is 0.38s. It may seem strange that in this last case having no time for braking, as was for the case in which FOV= +-5° & x = 0 m and the one in which FOV=+- 10° & x = + 0.83 m, a different time headway in the risky point is obtained, but in reality is not if considering what said before and so that depending on the maneuver and the position of the radar, the nearest point can be different and so has a different distance from the sensor (that is in any case related at maximum with the dimensions of the car), and so a time headway difference of 0.02 can be considered as negligible. In any case if the nearest point firstly sensed by the radar were the same even changing the sensor position, these time headways would be the same.
Finally for FOV = +-3° and x= - 0.83, 0 , +0.83 m the time difference & the time headway are respectively -0.62s & 1.41s, 0.50s & 0.39s, 1.62s & 0.41s. For clarity results are listed in Table 8.1 and Table 8.2.

Time difference in seconds	X = -0.83 m	X = 0 m	X = +0.83 m
FOV 3°	-0.62	0.50	1.62
FOV 5°	-0.93	0.22	1.39
FOV 10°	-1.59	-0.51	0.65

Table 8.1: Time difference for different radar configurations varying the FOV

Time headway in seconds in the risky point	X = -0.83 m	X = 0 m	X = +0.83 m
FOV 3°	1.41	0.39	0.41
FOV 5°	3.1	0.40	0.38
FOV 10°	Inf	1.08	0.40

Table 8.2: Time headway in the risky point for different radar configurations varying the FOV

The results show that increasing the FOV, depending on the set position, it is possible to increase the time difference between when the ego vehicle senses an obstacle (and so it can start to brake) and when the obstacle enters in a dangerous situation. This time difference increases almost linearly shifting the radar position from the right (closer to the cutting in car) to the left of the bumper, as shown in Figure 8.10 and the slope of

these lines do not changes changing the FOV. The time difference does not increase perfect linearly because, as said, changing the maneuver or the radar position the nearest point is not the same but since this difference is negligible it can be considered as a linear increasing.

Understood how the time difference and the time headway depend on the FOV, in Figure 8.11 and Figure 8.12 is shown how they depend on the velocity.

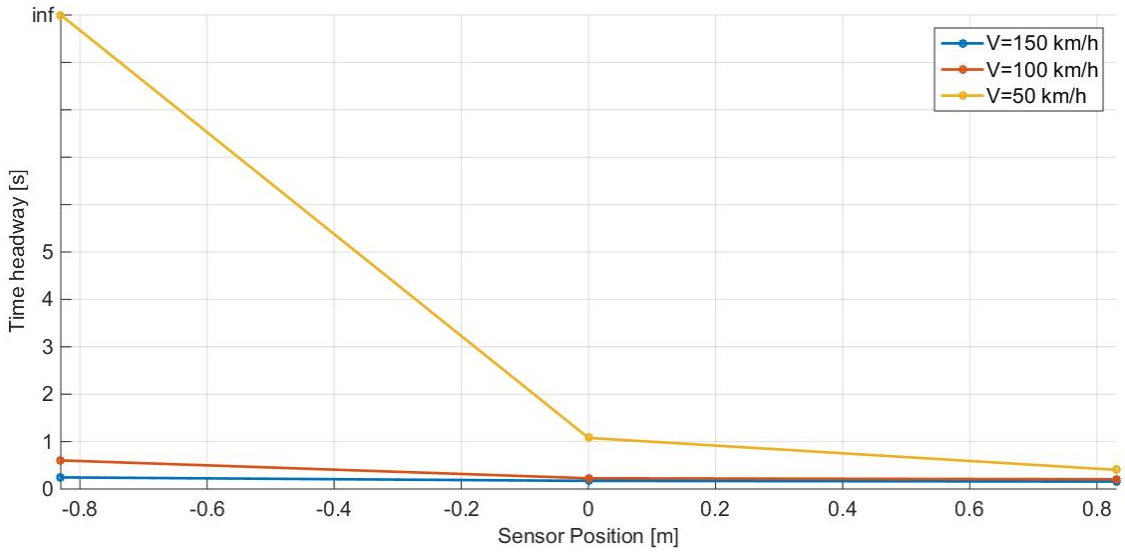

Figure 8.11: Time headway in the risky point considering three different sensor positions varying the speed

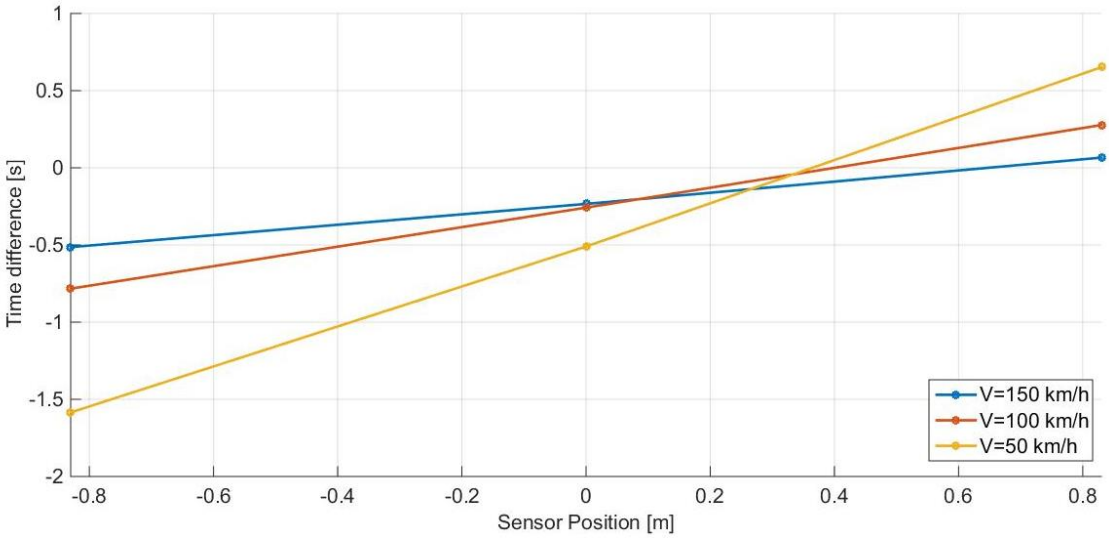

Figure 8.12: Time difference considering three different sensor positions varying the speed

In these simulations a FOV = +- 10° and an inclination angle α=3° are set. In this analysis it is possible to appreciate that increasing the speed, depending on the sensor position, the time headway will decrease since the time the cutting in car needs to reach the dangerous situation decreases and so less time has the ego vehicle to brake. Figure 8.11 shows that advantages are provided putting the sensor in the closest-to-object side of the car, but these advantages are almost negligible at high speeds. In fact if at 50 km/h the time headway evaluated in the risky point with the sensor in x=-0.83 and x=0.83 are respectively inf & 0.40s and so a considerable advantage has the shifting of the sensor position , at 100 km/h they are 0.60s & 0.20s having an advantage due to the shift of 0.4s, while at 150 km/h they are 0.24s & 0.16s with a gain of 0.08s that is negligible. Figure 8.12 shows that even in this case the time difference increases almost linearly moving from the right to left in the positioning of the sensor on the bumper but in this case changing the speed also the slope of the line will change. Results are listed in Table 8.3 and Table 8.4.

Time difference in seconds	X = -0.83 m	X = 0 m	X = +0.83 m
Speed 50 km/h	-1.59	-0.51	0.65
Speed 100 km/h	-0.78	-0.26	0.28
Speed 150 km/h	-0.51	-0.23	0.07

Table 8.3: Time difference for different radar configurations varying the speed

Time headway in seconds in the risky point	X = -0.83 m	X = 0 m	X = +0.83 m
Speed 50 km/h	Inf	1.08	0.40
Speed 100 km/h	0.60	0.23	0.20
Speed 150 km/h	0.24	0.17	0.16

Table 8.4: Time headway in the risky point for different radar configurations varying the speed

Finally, the dependence of the time headway in the risky point and of the time difference on the incidence angle α are shown in Figure 8.13 and Figure 8.14. In these simulations FOV= +- 5° and speed=50 km/h.

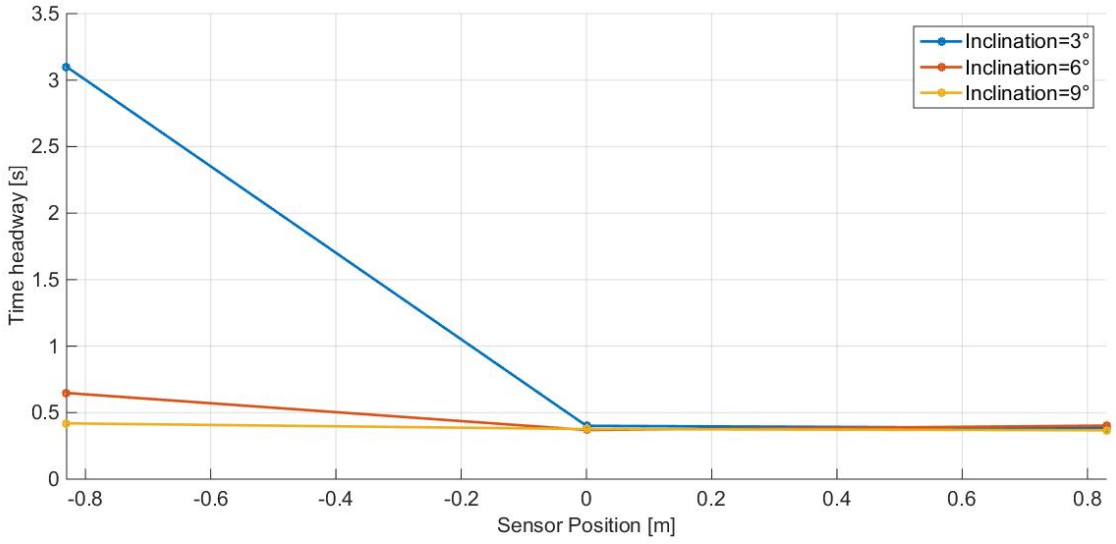

Figure 8.13: Time headway in the risky point considering three different sensor positions varying the inclination angle

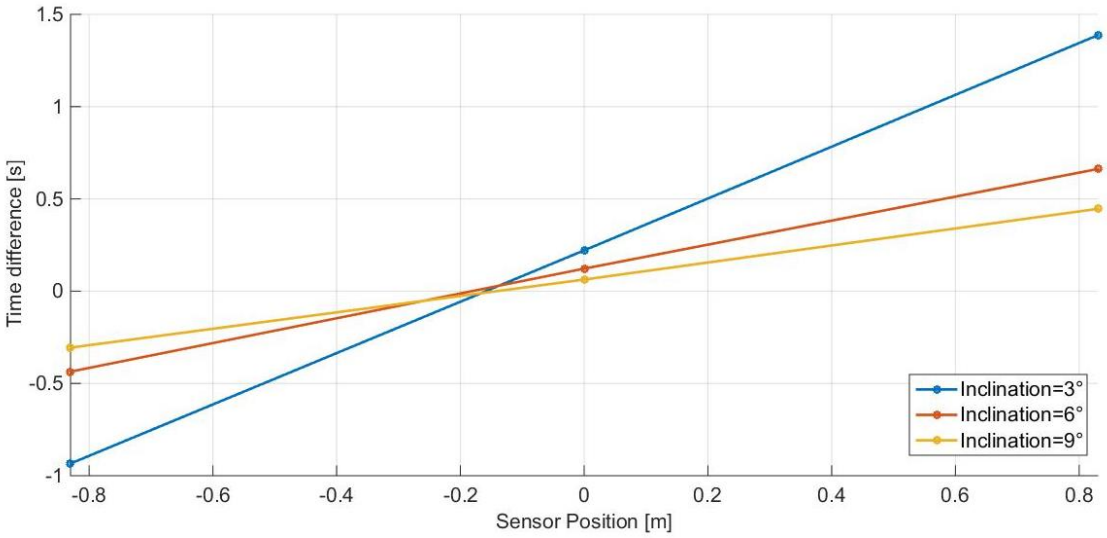

Figure 8.14: Time difference considering three different sensor positions varying the inclination angle

These results follow the same trends of the velocity dependent ones. Increasing α, depending on the sensor position, the time headway will decrease since the time that the cutting in car needs to reach the dangerous situation decreases and so less time has the ego vehicle to brake. Figure 8.13 shows that advantages are provided putting the sensor in the closest-to-object side of the car but these advantages are almost negligible at high inclination angles. In fact if at α=3° the time headway evaluated in the risky point with the sensor in x=-0.83 and x=0.83 are respectively 3.1s & 0.38s and so a considerable advantage has the shifting of the sensor position , at α=6° they are 0.65s & 0.40s having an advantage due to the shift of 0.25s, while at α =9° they are 0.42s & 0.37s with a gain of 0.05s that is negligible. Figure 8.14 shows that even in this case the time difference increases almost linearly moving from the right to left in the positioning of the sensor on the bumper but as for the velocity dependent case changing α also the slope of the line will change. Results are listed in Table 8.5 and Table 8.6.

Time difference in seconds	X = -0.83 m	X = 0 m	X = +0.83 m
Inclination angle 3°	-0.93	0.22	1.39
Inclination angle 6°	-0.44	0.12	0.66
Inclination angle 9°	-0.31	0.06	0.45

Table 8.5: Time difference for different radar configurations varying α

Time headway in seconds in the risky point	X = -0.83 m	X = 0 m	X = +0.83 m
Inclination angle 3°	3.1	0.40	0.38
Inclination angle 6°	0.65	0.37	0.40
Inclination angle 9°	0.42	0.38	0.37

Table 8.6: Time headway in the risky point for different radar configurations varying α

The analysis done confirms the dependence of the time headway on the FOV, on the inclination angle and on the speed. In order to tighten the dependence only to a variable some considerations can be done. First of all, once chosen the proper radar, the FOV is set and it is for long range detection aims around 3-5°. As the results demonstrate the dependence on α and on the speed follows the same trends and in fact they are both variables related to the aggressiveness of the maneuver. It is possible to evaluate this aggressiveness considering as parameter the time needed to the cutting in car to move from the starting position at the center of its lane to the dangerous one. This amount of time depends on the product between speed and sin(α). For small angle sin(α) can be approximated with α itself and since it is the case (think about an overtaking maneuver, the steer is turned of few degrees especially in highways), the aggressiveness will depend on the product between speed and α**.** In this case it possible to consider as variable of interest just that product. In fact, for example the amount of time needed to enter in the dangerous situation with a speed of 100 km/h and an inclination angle of 3° is almost the same of a maneuver done at 50 km/h but with an inclination of 6°. The time headway instead will not be the same since the velocity enters in the time headway formula while α doesn't. Considering that, is interesting evaluate the time headway in the risky point moving the speed and maintaining a fixed FOV as well as a fixed α**.** This simulation is done for four different speeds and for seven different sensor positions considering FOV= +- 5° and α=3°. The results are shown in Figure 8.15 and listed in Table 8.7.

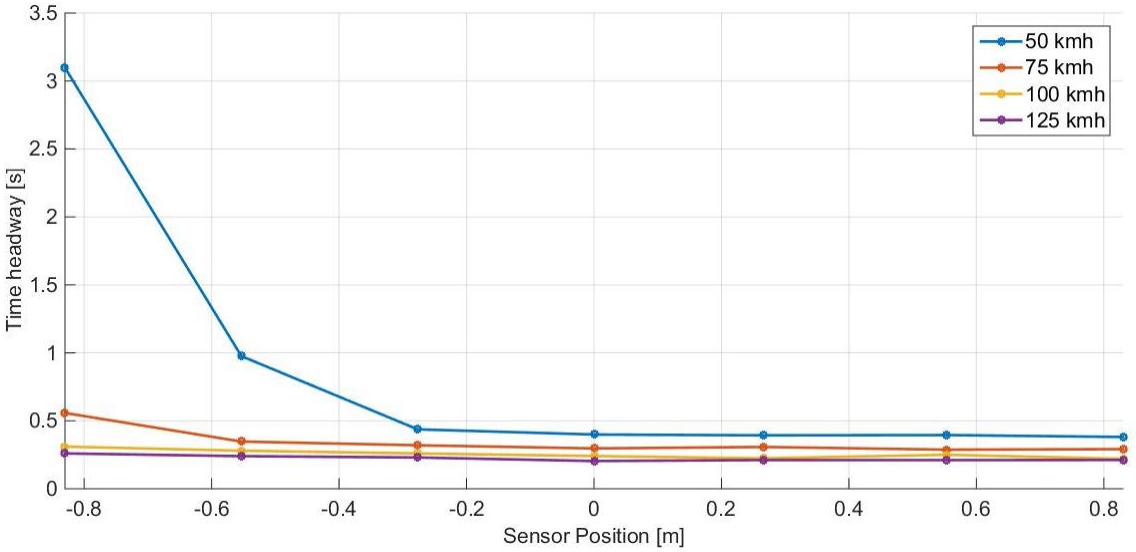

Figure 8.15: Time headway in the risky point considering seven different sensor positions varying the speed

TH [s] in the risky point	X =-0.830m	X =-0.553m	X =-0.277m	X =0m	X =0.277m	X =0.553m	X =0.830m
Speed 50 km/h	3.10	0.98	0.44	0.40	0.39	0.40	0.38
Speed 75 km/h	0.56	0.35	0.32	0.30	0.31	0.29	0.29
Speed 100 kmh	0.31	0.28	0.26	0.24	0.22	0.25	0.22
Speed 100 kmh	0.26	0.24	0.23	0.20	0.21	0.21	0.21

Table 8.7: Time headway in the risky point for different radar configurations varying the speed

The results confirm what seen previously and so that having a sensor set closer to the side in which the cut in maneuver is occurring gives benefits that are considerable if the cars are not moving with so high speeds (reasonably till 80 km/h). Instead having the sensor in the middle position or in the further side does not lead to significant loss in terms of time headway. These considerations can be rewritten and it is possible to say that, since the cut in maneuver could occur both from the right and from the left of the ego vehicle, there is no reason to move the sensor from the middle position but even doing that there is no significant time headway loss. In the case in which two sensors could be installed, instead a significant advantage at middle-low speeds would be

having these sensors set in the extreme sides of the front bumper.

Chapter 9

9. Conclusions

Advanced driver assistance systems improve safety and driver comfort representing a point of interest of all the carmakers which are spending a lot of efforts in order to provide even better systems aiming to reach complete autonomous vehicles. The starting point to guarantee this assistance is correctly perceive the surrounding environment giving information about traffic, road signs and obstacles even in risky circumstances. To reach this goal modern cars are equipped whit different sensors, each of them whit its peculiarity, pros and cons. The radar sensors are the ones most used especially when long range detection is needed, leveraging on their characteristics and ability to work even in environment in which other sensors could have problems. Nowadays in vehicle design also aesthetic is a crucial point and requires constraints. The sensors need to be hidden as much as possible to fit the design. Radar sensors are packaged in radomes and mounted behind plastic covers and bumpers, especially long-range radars used for adaptive cruise control and emergency braking. The signal emitted from the radar need to pass through different layers each of them attenuate the signal itself and demands a proper design in order to allow a correct transmission. The present study after introduced the main ADAS, the main pros and cons of the different sensors, focusing especially on the principle of working of automotive radars, provide a guide on

the integration of the radar in this multi-layers structure, mentioning the principal phenomena to be considered and simulating the benefits of using different materials. Polypropylene (PP) results as the best one for the covers that hide the sensor, since in PP absorption is negligible and also the percentage of power reflected back is less the one caused by the other material tested. Dimensioning of the different layers and the spacing between them are also to be considered during the design process, preferring thickness multiple of half the wavelength of the signal in such a way that back reflections occur in a constructive way being they in phase with the emitted signal. In the multi-layers structure in necessary to avoid paints and coatings that have metals in their composition, it could complete destroy the transmission. Considerations about geometry and covers shape are also performed, reaching the conclusion that flat surfaces over the radar are preferable since is easier to evaluate the beam's deflection. The position of the radar is evaluated through a simulator, considering its limits, especially focusing on the horizontal shifting of the sensor in the presence of a cut-in maneuver. In this case, if only one radar is present, there is no reason to move it from the middle position of the car's bumper, but if two different sensors are used, putting them near to the extreme side of the bumper provides significant advantages in terms of time headway, but mainly if the maneuvers occur at middle-low speeds.

10. Bibliography

[1] C. Ushemadzoro, K. Peter and C. Shawn, "From Antenna Design to High Fidelity, Full Physics Automotive Radar Sensor Corner Case Simulation," 2018.

[2] U. Chipengo, "Full physics simulation of terrain-adaptive 77 GHz automotive radar for early pedestrian detection," 2019.

[3] [Online]. Available: https://www.lexus.eu/discover-lexus/technology/lexus-safety/front-cross-traffic-alert. [Accessed 25 11 2022].

[4] [Online]. Available: https://www.polestar.com/it-ch/manual/polestar-2/2021/article/Avvertimento-e-freno-automatico-in-retromarcia*. [Accessed 25 11 2022].

[5] G. L. Zagaria and F. Caviggioli, "Veicoli a guida autonoma: Analisi Brevettuale," Turin, 2019.

[6] K. Ohguchi, M. Shono and M. Kishida, "79GHz Band Ultra-Wideband Automotive Radar," 2013.

[7] [Online]. Available: https://www.ebay.it/b/Accessori-per-Fiat-Tipo-Station-Wagon/82099/bn_7012232162. [Accessed 25 11 2022].

[8] D. D. Crescenzo, D. Dardari, G. Pasolini and A. Guerra, "Radar perimetrali per applicazioni automotive," Bologna, 2021.

[9] H. Winner, S. Hakuli, F. Lotz and C. Singer, Handbook of Driver Assistance Systems, Springer International Publishing Switzerland, 2016.

[10] R. Abou-Jaoude, "ACC radar sensor technology, test requirements, and test solutions," *IEEE Transactions on Intelligent Transportation Systems,* 2003.

[11] M. Parker, Digital Signal Processing 101 (Second Edition), 2017.

[12] I. Cesar, "The fundamentals of millimeter wave sensors," 2017.

[13] S. M. Patole, M. Torlak, D. Wang and M. Ali, "Automotive radars: A review of signal processing techniques," *IEEE Signal Processing Magazine,* 2017.

[14] R. Sandeep, "Introduction to mmWave sensing: FMCW radars," 2017.

[15] R. K. and R. K., "Moving from Legacy 24 GHz to State-of-the-Art 77-GHz Radar,"

2018.

[16] J. Hasch, E. Topak, R. Schnabel, T. Zwick, R. Weigel and C. Waldschmidt, "Millimeter-Wave Technology for Automotive Radar Sensors in the 77 GHz Frequency Band," *IEEE Transactions on Microwave Theory and Techniques,* 2012.

[17] [Online]. Available: https://it.m.wikipedia.org/wiki/File:Doppler_Weather_Radar_-_NOAA.jpg. [Accessed 25 11 2022].

[18] [Online]. Available: https://www.ansys.com/it-it/blog/new-hfss-sbr-technology-in-ansys-2021-r2. [Accessed 25 11 2022].

[19] F. Fitzek and R. H. Rasshofer, "Automotive Radome Design - Reflection Reduction of Stratified Media," *IEEE Antennas and Wireless Propagation Letters,* 2009.

[20] Y. Xiao, F. Norouzian, E. G. Hoare, E. Marchetti, M. Gashinova and M. Cherniakov, "Modeling and Experiment Verification of Transmissivity of Low-THz Radar Signal Through Vehicle Infrastructure," *IEEE Sensors Journal,* no. 2020.

[21] H. Chen, L. Huang and M. Tong, "Frequency selective surface in millimeter-wave automotive radar radome applications," *Progress in Electromagnetic Research Symposium (PIERS),* 2016.

[22] M. M. S. Hossain, "Wideband Radomes for Millimeter-Wave Automotive Radars," *IEEE Transactions on Antennas and Propagation,* 2022.

[23] AG Infineon Technologies, "Radar wave propagation through materials," 2020.

[24] [Online]. Available: https://www.vedantu.com/question-answer/derive-the-following-expression-for-the-class-12-physics-cbse-5fa113598ab42b31479c2f44. [Accessed 25 11 2022].

[25] [Online]. Available: https://www.toppr.com/guides/physics/ray-optics-and-optical-instruments/refraction-at-spherical-surface-and-by-lenses/. [Accessed 25 11 2022].